STRUCTURAL BIOLOGY

Receptor-specific recognition of NPY peptides revealed by structures of NPY receptors

Tingting Tang[1,2]†, Qiuxiang Tan[2]†, Shuo Han[2]†, Anne Diemar[3]†, Kristin Löbner[3], Hongyu Wang[2,4], Corinna Schüß[3], Victoria Behr[3], Karin Mörl[3], Mu Wang[2,5], Xiaojing Chu[2], Cuiying Yi[2], Max Keller[6], Jacob Kofoed[7], Steffen Reedtz-Runge[7], Anette Kaiser[3]*, Annette G. Beck-Sickinger[3]*, Qiang Zhao[2,4,8]*, Beili Wu[1,2,4,5]*

In response to three highly conserved neuropeptides, neuropeptide Y (NPY), peptide YY, and pancreatic polypeptide (PP), four G protein–coupled receptors mediate multiple essential physiological processes, such as food intake, vasoconstriction, sedation, and memory retention. Here, we report the structures of the human Y_1, Y_2, and Y_4 receptors in complex with NPY or PP, and the G_{i1} protein. These structures reveal distinct binding poses of the peptide upon coupling to different receptors, reflecting the importance of the conformational plasticity of the peptide in recognizing the NPY receptors. The N terminus of the peptide forms extensive interactions with the Y_1 receptor, but not with the Y_2 and Y_4 receptors. Supported by mutagenesis and functional studies, subtype-specific interactions between the receptors and peptides were further observed. These findings provide insight into key factors that govern NPY signal recognition and transduction, and would enable development of selective drugs.

INTRODUCTION

Neuropeptide Y (NPY), peptide YY (PYY), and pancreatic polypeptide (PP) are 36-residue C-terminally amidated neuropeptides that share a similar sequence (*1*, *2*). Despite recognizing the same set of peptide agonists, the NPY receptors differ in their ligand-binding preference (*3*). The Y_4 receptor (Y_4R) is the only member of this family, with PP as its most potent endogenous agonist, whereas the preferred agonists for the Y_1 receptor (Y_1R), Y_2 receptor (Y_2R), and Y_5 receptor (Y_5R) are NPY and PYY. The poor sequence identity (27 to 32%) between these three receptors makes them the most divergent heterotrimeric guanine nucleotide-binding protein (G protein)–coupled receptors (GPCRs) that interact with the same family of homologous peptide ligands (*2*, *4*). This suggests receptor-specific recognition of the NPY peptides. Y_1R and Y_4R require the full-length N terminus of NPY for full agonist activity, while Y_2R can bind N-terminally truncated NPY and PYY with high affinity and Y_5R accepts peptides with deletion of the first residue (*5*). Furthermore, Y_1R appears to form interactions with more residues at the peptide C terminus than Y_2R (*6*). These findings suggest diversity of the NPY binding mode at its receptors, which is essential for understanding the molecular mechanisms of signal recognition and transduction of the NPY system and provides the molecular basis for developing selective drugs that target different NPY receptors. However, the molecular details that define the distinct recognition patterns between the receptors and peptides remain unknown.

The NPY receptors are largely involved in appetite regulation but differ in their physiological roles. Y_1R and Y_5R exert an appetite-stimulating effect (*7*), while Y_2R and Y_4R inhibit food intake (*8*, *9*). Many efforts have been made to develop drugs to treat obesity by regulating this system (*10*, *11*), and several peptide ligands with improved selectivity have been developed (*12*–*14*). However, the design of efficient and stabilized drugs, including small-molecule agonists, is limited by the lack of structural understanding, in particular regarding the subtle conformational changes in the C-terminal region of the peptide (*15*, *16*) and the unclear role of the peptide N terminus. To provide molecular details that define the recognition of NPY by different NPY receptors and to enable structure-based drug design, we determined the structures of both Y_1R and Y_2R in complex with NPY and heterotrimeric G_{i1} protein as well as Y_4R bound to PP and G_{i1} using cryo–electron microscopy (cryo-EM) single-particle analysis. Combined with binding and functional studies, the structures offer structural and mechanistic insights into NPY signal recognition and transduction.

RESULTS AND DISCUSSION

Active structures of G_{i1}-bound YRs

To facilitate expression and purification of the NPY peptide– and G_{i1}-bound YR complexes, a hemagglutinin (HA) signal peptide and a Flag epitope tag were added to the N termini of the receptors, and the C-terminal residues (R341-I384 in Y_1R; S354-V381 in Y_2R; S343-I375 in Y_4R) were replaced with a twin-strep-tag. Functional assays demonstrate that these modifications have little effect on receptor signaling (table S1). The NPY-Y_1R-G_{i1}, NPY-Y_2R-G_{i1}, and PP-Y_4R-G_{i1} structures were determined with an overall resolution of 3.2, 3.4, and 3.0 Å, respectively (Fig. 1, fig. S1, and table S2). The resulting density maps allowed unambiguous modeling of side chains for most of the residues in the receptors, peptide agonists, and G protein in the three structures, except for the residues 10 to 12 in the middle linker region of NPY and PP, which lack contact with the receptors (fig. S2).

Upon binding to the NPY peptide and G_{i1}, Y_1R, Y_2R, and Y_4R are structurally similar with C_α root mean square deviation of 1.3 Å

[1]School of Pharmaceutical Science and Technology, Hangzhou Institute for Advanced Study, UCAS, Hangzhou, China. [2]CAS Key Laboratory of Receptor Research, State Key Laboratory of Drug Research, Shanghai Institute of Materia Medica, Chinese Academy of Sciences, Shanghai, China. [3]Institute of Biochemistry, Faculty of Life Sciences, Leipzig University, Leipzig, Germany. [4]University of Chinese Academy of Sciences, Beijing, China. [5]School of Life Science and Technology, ShanghaiTech University, Shanghai, China. [6]Pharmaceutical/Medicinal Chemistry II, Institute of Pharmacy, University of Regensburg, Regensburg, Germany. [7]Novo Nordisk A/S, Novo Nordisk Park, Måløv, Denmark. [8]Zhongshan Institute for Drug Discovery, Shanghai Institute of Materia Medica, Chinese Academy of Sciences, Zhongshan, China.
*Corresponding author. Email: anette.kaiser@uni-leipzig.de (A.K.); abeck-sickinger@uni-leipzig.de (A.G.B.-S.); zhaoq@simm.ac.cn (Q.Z.); beiliwu@simm.ac.cn (B.W.)
†These authors contributed equally to this work.

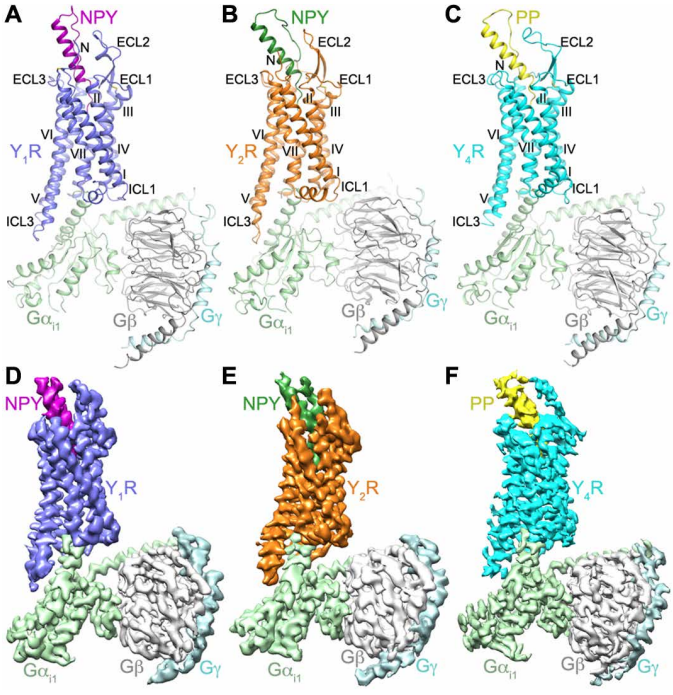

Fig. 1. Structures and cryo-EM maps of NPY/PP-YR-G_{i1} complexes. (**A**) Structure of the NPY-Y_1R-G_{i1} complex. Y_1R, NPY, $G\alpha_{i1}$, Gβ, and Gγ are colored blue, purple, light green, gray, and light cyan, respectively. (**B**) Structure of the NPY-Y_2R-G_{i1} complex. Y_2R, NPY, $G\alpha_{i1}$, Gβ, and Gγ are colored orange, green, light green, gray, and light cyan, respectively. (**C**) Structure of the PP-Y_4R-G_{i1} complex. Y_4R, PP, $G\alpha_{i1}$, Gβ, and Gγ are colored cyan, yellow, light green, gray, and light cyan, respectively. The structures are shown in cartoon representation. The disulfide bonds are shown as yellow sticks. (**D** to **F**) Cryo-EM maps of the NPY/PP-YR-G_{i1} structures, colored according to chains. (D) NPY-Y_1R-G_{i1}; (E) NPY-Y_2R-G_{i1}; (F) PP-Y_4R-G_{i1}.

(Y_1R versus Y_2R) and 1.6 Å (Y_1R versus Y_4R). The receptors share common structural features with the previously determined active structures of class A GPCRs (Fig. 1). Because of a spatial hindrance caused by the agonist, the highly conserved "toggle switch" (*17*) residue $W^{6.48}$ [superscript on residue indicates Ballesteros-Weinstein nomenclature (*18*)] in the three receptors displays a rotamer conformational change, with its side chain shifting toward the receptor intracellular surface compared to that in our previously determined antagonist-bound structures of Y_1R (*16*) and Y_2R (fig. S3, A to C) (*19*). This shift forces another conserved residue $F^{6.44}$ to move away from the central axis of the receptor helical bundle and further triggers an outward movement of the intracellular half of helix VI, which is required for G protein binding.

Comparison of the active and inactive structures of YRs reveals a structural rearrangement in the intracellular region of the receptors, including the signature outward shift of helix VI (~9 Å) and an inward movement of helix VII (~4 Å), which generate a binding cavity for the G protein (fig. S3, D to F). The three NPY/PP-YR-G_{i1} structures and other G_i-bound class A GPCR structures (*20*–*24*) exhibit a similar binding pocket to accommodate the α subunit of G_i, where the backbone conformations overlay for both the receptor helical bundle and the C terminus of the α5 helix in $G\alpha_i$ (fig. S3H). In contrast to the similar positioning of the α5 C terminus, the N terminus of this helix shifts toward the third intracellular loop (ICL3) of the receptor in the NPY-Y_2R-G_{i1} structure relative to the Y_1R and Y_4R complexes. This positional difference is accompanied by a translational movement of the rest of the Gα subunit and the Gβ and Gγ subunits (fig. S3G).

Binding site of NPY peptides in YRs

In the structures of NPY-Y_1R-G_{i1}, NPY-Y_2R-G_{i1}, and PP-Y_4R-G_{i1}, the agonists NPY and PP occupy a large binding pocket shaped by the extracellular loops and helices II to VII of the receptors (Fig. 2, A to F; fig. S4; and table S3). The peptide ligands adopt a hairpin-like fold with the unstructured N terminus (residues 1 to 10) and the α helix (residues 14 to 31) in the C-terminal region running antiparallel. The unstructured C-terminal pentapeptide T32-Y36 in the peptides, which is essential for binding to all NPY receptors (*2*, *25*), penetrates into the ligand-binding pocket within the receptor transmembrane helical bundle (Fig. 2, A to C). The α-helical region leans against the receptor N terminus and makes extensive contacts with the second and third extracellular loops (ECL2 and ECL3), while the peptide N terminus points toward the extracellular tip of helix V (Fig. 2, D to F).

The hairpin-like fold that PP adopts in the PP-Y_4R-G_{i1} complex is similar to the previously determined crystal structure of PP, which is the so-called "PP-fold" (*26*). However, this fold was clearly not observed for NPY, either in solution or in the lipid-bound state by nuclear magnetic resonance (NMR)–based (*27*, *28*), electron paramagnetic resonance (EPR)–based (*29*), or fluorescence resonance energy transfer (FRET)–based studies (*30*); accordingly, this conformation of NPY is enforced only in the respective receptor binding pockets. Despite distinct binding modes and the different functional significance of the peptide N terminus for the NPY peptide binding to Y_1R, Y_2R, and Y_4R as discussed below, residues P2 to P8 of the peptides form extensive contacts with the segment Y20-I31 in the α helix, mainly through hydrophobic interactions between three prolines, P2, P5, and P8, and two aromatic residues, Y20 and Y27 (Fig. 2, A to C). Previously reported reductions in the binding affinity for the alanine variants of these prolines (*31*) and tyrosines (*2*, *5*) suggest that the intra-peptide interactions, which stabilize the hairpin-like fold of the NPY peptides, are essential for high-affinity binding of the peptide agonists to the NPY receptors.

Although Y_1R, Y_2R, and Y_5R are structurally divergent, with only 27 to 32% sequence identity, these receptors bind NPY with (sub)nanomolar affinities, suggesting that the peptide ligand may adopt distinct conformations upon binding to different receptors (*5*). The structures of NPY-bound Y_1R and Y_2R reveal different binding poses of NPY. The largest variation occurs at the N terminus of the peptide agonist. When bound to Y_2R, the peptide N terminus stacks on top of the C-terminal region of ECL2, while in contrast, the N terminus of NPY shifts toward ECL3 and binds deeper within the helical bundle in Y_1R (Fig. 2, A, B, D, E, and G). Furthermore, the α helix in the peptide C-terminal region rotates counterclockwise (extracellular view) by about 45° and moves closer to the receptor N terminus and ECL3 in the NPY-Y_1R-G_{i1} structure relative to the NPY-bound Y_2R structure (Fig. 2G). Close inspection of the two structures revealed a spatial hindrance caused by the extra one-turn helix of residues D181-Q185 in ECL2 of Y_1R, which pushes the N terminus and the α-helical segment around residue Y27 of NPY away from ECL2 (Fig. 2G). In addition, the replacement of the Y_2R residue $Y303^{7.31}$ with $H298^{7.31}$ in Y_1R, which has a smaller side chain, further facilitates the movement of the peptide toward ECL3 (Fig. 2H). In contrast to the diverse binding behaviors of the N-terminal region

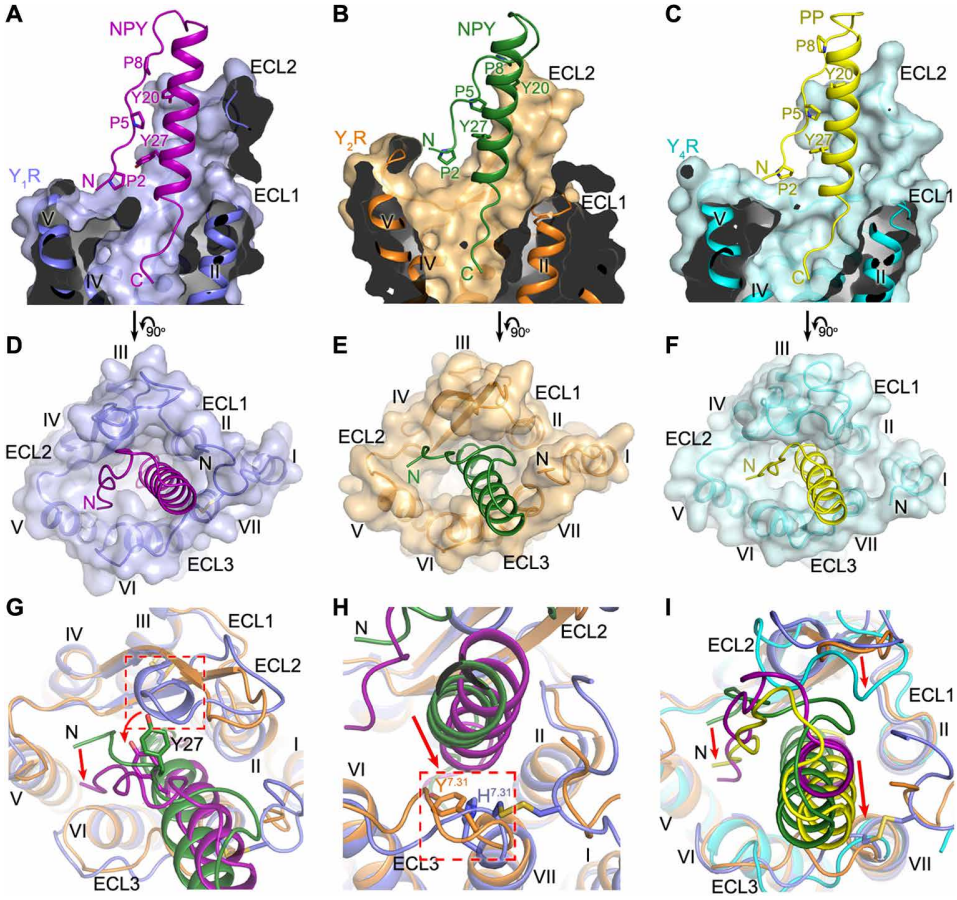

Fig. 2. Binding site of NPY peptides in YRs. (**A** to **C**) Cutaway view of the NPY/PP-binding pocket in YRs. (A) The NPY-Y_1R-G_{i1} structure is shown in cartoon representation and colored blue (Y_1R) and purple (NPY). The receptor is also shown as surface. (B) The NPY-Y_2R-G_{i1} structure is colored orange (Y_2R) and green (NPY). (C) The PP-Y_4R-G_{i1} structure is colored cyan (Y_4R) and yellow (PP). (**D** to **F**) Extracellular view of the NPY/PP-binding pocket in YRs. (D) NPY-Y_1R-G_{i1}; (E) NPY-Y_2R-G_{i1}; (F) PP-Y_4R-G_{i1}. (**G** and **H**) Comparison of the binding pose of NPY at Y_1R and Y_2R. (G) The red arrows indicate the conformational changes of the peptide N terminus and the peptide residue Y27 in the NPY-Y_1R-G_{i1} structure relative to the NPY-Y_2R-G_{i1} structure. The extra one-turn helix in ECL2 of Y_1R, which induces the movement of NPY toward ECL3, is highlighted by a red dashed box. (H) The red arrow indicates the movement of the α-helical region of NPY in the NPY-Y_1R-G_{i1} structure relative to the NPY-Y_2R-G_{i1} structure. The residues at position 7.31 ($H^{7.31}$ in Y_1R, $Y^{7.31}$ in Y_2R), which facilitate the movement of NPY, are highlighted by a red dashed box. (**I**) Comparison of the binding poses of NPY in Y_1R/Y_2R and PP in Y_4R. The red arrows indicate the movements of the N terminus and α-helical region of PP and the receptor ECL2 in the PP-Y_4R-G_{i1} structure relative to the NPY-Y_1R-G_{i1} and NPY-Y_2R-G_{i1} structures.

and α helix of NPY at Y_1R and Y_2R, the C terminus of the peptide agonist occupies a similar binding site at the bottom of the ligand-binding pocket in both receptors (Fig. 2, A and B). These observations demonstrate that NPY is structurally flexible and can adapt to different receptors by adjusting its conformation.

Compared to NPY at Y_1R and Y_2R, the closely related peptide PP adopts a similar binding pose upon binding to Y_4R, with its C terminus occupying a similar binding site within the transmembrane helical bundle and the N terminus aligning well with that of NPY in Y_1R (Fig. 2, C, F, and I). Despite these similarities, the N-terminal loop and α helix of PP slightly shift toward ECL3, which is associated with an inward movement of ECL2 in Y_4R (Fig. 2I). This difference further highlights the diversity of the NPY peptide binding mode.

Validation of NanoBRET-based binding assays for Y_1R, Y_2R, and Y_4R

To investigate the ligand-binding behavior of the YRs, we carried out a ligand-binding assay by means of a recently developed NanoBRET-based methodology (*32*, *33*), using a nanoluciferase fused to the N terminus of the receptor as energy donor, and a fluorophore-tagged peptide ligand as acceptor. This provides a homogeneous, wash-free assay setup that can directly report about ligand affinities over many orders of magnitude and at the same time is sensitive to conformational changes in the binding pocket. We verified the wild type–like properties of the tagged peptide and receptor constructs by cross-validation using receptor activation assays and radioligand binding (table S4). Two clearly separated affinity states for the peptide binding to the receptors were observed (fig. S5). We confirmed that the biphasic nature of the binding curves is not an artefact of peptide labeling by repositioning of the fluorophore (fig. S5, A, E, and I). The two affinity states for the fluorophore-labeled NPY at Y_1R had similar bioluminescence energy transfer (BRET) windows and dissociation constants of $K_{D,1}$ = 4.0 nM and $K_{D,2}$ = 126 nM, respectively (fig. S5A and table S4). For Y_2R, the affinity differences were even more pronounced with a high-affinity, but very low-BRET state with $K_{D,1}$ of 0.12 nM, and a low-affinity, but high-BRET

state with $K_{D,2}$ of 349 nM (fig. S5E and table S4). The high-affinity state at Y_4R had a $K_{D,1}$ of 18 nM, and the low-affinity state showed poor affinity of over 1 μM in isolated membranes (fig. S5I). In intact cells, the population and thus the BRET window of the high-affinity state of Y_4R were markedly increased with the $K_{D,1}$ remaining similar (26 nM; fig. S5J), while binding behavior at Y_1R and Y_2R was very similar in isolated membranes and intact cells (fig. S5, A, B, E, and F). We therefore chose to measure ligand binding at isolated membranes for Y_1R and Y_2R, but in intact cells for Y_4R.

We further looked into the characteristics of the two affinity states. For Y_2R, we confirmed the specificity of the low-affinity binding by displacement assays with NPY and the antagonist JNJ-31020028 (fig. S5, M and N). While JNJ-31020028 had essentially the same affinity (K_i) in both states, as expected for a neutral antagonist, the K_i of unlabeled NPY differed greatly when displaced from the high- and low-affinity states, respectively. We hence speculated that the G protein might allosterically stabilize the high-affinity state of Y_2R and potentially act in a similar manner at Y_1R and Y_4R. To investigate this, we measured ligand binding at receptor constructs carrying a flavodoxin or T4 lysozyme (T4L) in their ICL3 that sterically blocks the access of the G protein (fig. S5, D, H, and L). These constructs had been developed before to crystallize Y_1R (*16*) and Y_2R (*19*) in complex with small-molecule antagonists. For Y_4R, we generated six fusion constructs with different insertion sites. The Y_2R-flavodoxin fusion construct was completely devoid of a high-affinity state (fig. S5G). At Y_1R, the high-affinity state was markedly reduced for the ICL3-T4L fusion construct (wild type: 50 ± 4% of total netBRET; ICL3-T4L fusion construct: 29 ± 5% of total netBRET) and the Hill-Slope in a four-parameter model would approach unity (wild type: $n_H = 0.55 \pm 0.03$; ICL3-T4L fusion construct: $n_H = 0.73 \pm 0.03$; fig. S5C), in agreement with the G protein being required to stabilize the high-affinity states at these receptors. In contrast, the G protein is not required to stabilize the high-affinity state of Y_4R. Despite that all tested fusion constructs were unable to activate the G protein (fig. S5L), ligand binding was only marginally affected (fig. S5K), suggesting that another cytosolic protein enhances high-affinity binding to Y_4R in intact cells over isolated membranes (fig. S5, I and J). We hence suggest that NPY initially binds with a moderate affinity of over 100 nM to the extracellular region of Y_1R and Y_2R as discussed below, and the affinity of the peptide is then enhanced by adopting the structurally observed, deep binding pose, which is stabilized by G protein coupling. At Y_4R, high-affinity binding of PP is possible without allosteric stabilization of the G protein.

Different binding modes of the NPY N terminus

It has been well known that the N terminus of the NPY peptide contributes differently to the binding of the peptide to the different NPY receptor subtypes (*2*, *5*). However, the molecular details that define the various binding modes of the peptide N-terminal region have remained unknown. In the NPY-Y_2R-G_{i1} structure, the N-terminal half of NPY makes only a few contacts with the receptor. Residue Y1 of NPY approaches the C-terminal region of ECL2 in Y_2R, with its positively charged N-terminal amino group adjacent to the residues E210 and E211 at the hinge region between the β-hairpin of ECL2 and helix V (Fig. 3B). Additional interactions are observed for the NPY residues P5 and P8, which form hydrophobic contacts with residues I194 and I195 in ECL2, respectively. This was supported by mutagenesis of the residue I194 [which also interacts with L24 in the α helix of NPY (see below)], which reduced the potency of NPY in inducing inositol phosphate (IP) accumulation by 15-fold when replaced by asparagine (*15*). However, mutagenesis of residues I195, E210, and E211 to alanine did not measurably impede signaling of Y_2R (Fig. 3N and table S1) or reduce high-affinity binding (Fig. 4D, fig. S6, and table S4), suggesting that these interactions are not critical for function. This is consistent with the high dynamics of both the N-terminal part of NPY and the surrounding receptor regions, which is reflected by the relatively low local resolution in this region (figs. S2B and S3J). Except for these weak interactions, the N-terminal segment and middle region of NPY (residues Y1 to Y20) lack contact with the receptor (fig. S4, D and E, and table S3). These structural features align well with previous findings that the N-terminally truncated NPY analogs, NPY(3–36), NPY(13–36), NPY(18–36), and even NPY(22–36), can bind to Y_2R with subnanomolar affinity (*5*).

In contrast to the poor contribution of the N terminus of NPY to Y_2R binding, the N-terminal residues of the peptide play a crucial role in mediating Y_1R coupling. This was reflected by a more than 50-fold reduction of affinity and activity, respectively, of the truncated analogs NPY(2–36) and NPY(3–36) at Y_1R (*16*, *31*). The N-terminal part of NPY is very well defined in its structural position as judged by the local resolution of the cryo-EM map and three-dimensional (3D) variability analysis of the cryo-EM data, which shows less motions of the peptide N terminus and neighboring receptor regions in the Y_1R complex than in the Y_2R complex, suggesting limited dynamics of this region in contrast to that at Y_2R (figs. S2A and S3I and movie S1). The residue Y1 of NPY forms extensive contacts with the receptor in the NPY-bound Y_1R structure. It lies in a small cavity formed by ECL2 and the extracellular tips of helices V and VI of the receptor, with its positively charged N-terminal amino group forming a salt bridge with the acidic residue $D205^{5.32}$ in helix V and the side-chain hydroxyl making an additional polar contact with the side chain of D200 in ECL2 (Fig. 3A). Furthermore, the bulky side chain of the Y1 residue makes hydrophobic contacts with the side chains of F199, $R208^{5.35}$, and $F286^{6.58}$ (Fig. 3A). The importance of these interactions for peptide agonist recognition is supported by our mutagenesis studies, in which the alanine replacements of F199, D200, and $F286^{6.58}$ decreased NPY potency by 4- to 20-fold in the IP accumulation assay (Fig. 3M and table S1). The functional contribution of the key residues within the NPY binding pocket of Y_1R and Y_2R was further investigated using the NanoBRET-based binding assay. We focused on changes in the high-affinity state, as this likely reflects the functional role of these residues in stabilizing the G protein binding and signaling as outlined above. Using this assay, a reduced BRET window ($BRET_{max}$) of the high-affinity state was observed for the Y_1R mutants D200A, $R208^{5.35}A$, and $F286^{6.58}A$ (Fig. 4A, fig. S6, and table S4), suggesting a destabilization of the high-affinity peptide–receptor–G protein complex. These data further underline the importance of the interactions between Y_1R and the N terminus of NPY in stabilizing the peptide in a proper binding pose that is essential for full agonist activity.

Previous investigation of centrally truncated or structurally constrained analogs of NPY showed that a certain length between the N- and C-terminal fragments was required for retaining high-affinity binding to Y_1R (*34*). This could be explained by the importance of the relative positioning of the N and C termini of the peptide agonist in mediating the recognition between Y_1R and NPY. In the NPY-Y_1R-G_{i1} structure, residues Y1 and P2 at the peptide N terminus connect to the C-terminal residues L30 and R33 using the receptor

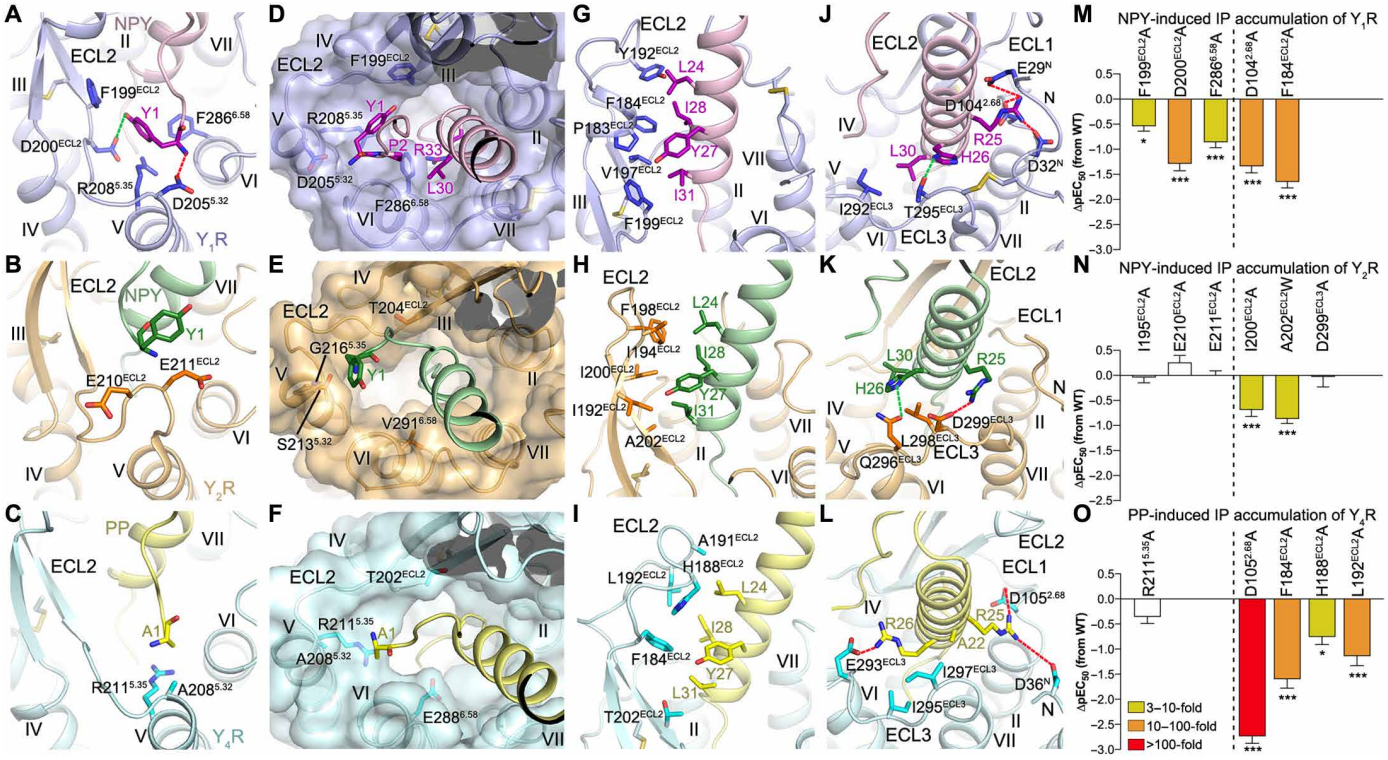

Fig. 3. Interactions between YR and the N terminus and α-helical region of the NPY peptide. (**A** to **C**) Interactions between YR and the N-terminal residue Y/A1 of the NPY peptide. The salt bridges and hydrogen bonds are shown as red and green dashed lines, respectively. (**D** to **F**) Binding site for the N terminus of the NPY peptide in the YRs. The receptors are shown in both cartoon and surface representations. (**G** to **L**) Interactions between the NPY peptide and the extracellular loops of the YRs. (A, D, G, and J) NPY-Y_1R-G_{i1}; (B, E, H, and K) NPY-Y_2R-G_{i1}; (C, F, I, and L) PP-Y_4R-G_{i1}. (**M** to **O**) NPY/PP-induced IP accumulation of YRs. (M) Y_1R mutants; (N) Y_2R mutants; (O) Y_4R mutants. Bars represent differences in calculated peptide potency (pEC_{50}) for each mutant relative to the wild-type (WT) receptor. Data are colored according to the extent of effect (EC_{50} ratio). Data are means ± SEM from at least three independent experiments performed in technical triplicate. *$P < 0.01$; ***$P < 0.0001$ by one-way analysis of variance followed by Dunnett's post-test, compared with the response of the WT receptor. See table S1 for detailed statistical evaluation and expression level. The mutants on the left side of the dashed line are for the receptor residues involved in interaction with the N-terminal residue Y1/A1 of the NPY peptide, while the mutants on the right side are for the residues from the receptor extracellular loops.

residue F286$^{6.58}$ as a "bridge" (Fig. 3D). These residues, located at the entrance to the narrow ligand-binding pocket that accommodates the C terminus of NPY, form an interaction core to cause the binding pocket to close and lock the peptide C terminus into its binding position. The residue F286$^{6.58}$, which plays a major role in holding the interaction core together, was found to be important for peptide agonist binding, with its alanine mutation leading to a marked loss of NPY and PYY binding (*35*–*37*). These findings indicate that the N terminus of NPY plays a critical role in stabilizing the optimal contacts between Y_1R and the agonist through its interactions with the receptor and peptide C terminus.

Comparison of the NPY-bound Y_1R and Y_2R structures reveals that most of the key Y_1R residues within the binding site for the NPY residue Y1 are not conserved in Y_2R (Fig. 3E). D205$^{5.32}$ is substituted by a serine in Y_2R, which abolishes the ionic interaction with the positively charged peptide N terminus. The Y_1R residues F199, R208$^{5.35}$, and F286$^{6.58}$ that provide a binding cavity for the bulky side chain of Y1 are replaced with residues having short side chains, T204, G216$^{5.35}$, and V291$^{6.58}$, in Y_2R. These differences exclude the possibility of the same site in Y_2R accommodating the N terminus of NPY and result in a more open binding pocket for the peptide C terminus (Fig. 3E). Furthermore, the Y_2R residues G209-K212 at the hinge region between the β-hairpin of ECL2 and helix V form a protrusion, which potentially prevents the entrance of the peptide N terminus into the ligand-binding pocket within the receptor helical bundle (fig. S7A). Such a protrusion of ECL2 is absent in Y_1R, allowing deep access of the N terminus of NPY.

Similar to Y_1R, Y_4R also lacks the bulge in ECL2 and allows the N terminus of the peptide agonist to reach a binding site similar to that in Y_1R (fig. S7A). However, the N-terminal residue A1 of PP forms only limited contacts with Y_4R (Fig. 3C and table S3). As observed in Y_2R, the resolution of the cryo-EM map is relatively low at this site in Y_4R and PP, consistent with greater structural flexibility and a less defined interaction network (figs. S2C and S3K), which are further reflected by the 3D variability analysis of the cryo-EM data that shows large motions in this region of the Y_4R complex (movie S1). This is in line with the limited functional impairment of the N-terminally truncated PP(2–36) at Y_4R (*38*). In addition, this site in Y_4R would not provide a strong binding environment for the N-terminal residue Y1 of NPY, as the Y_1R residue D205$^{5.32}$ is replaced with an alanine in Y_4R and the two bulky Y_1R residues F199 and F286$^{6.58}$ are replaced with T202 and E288$^{6.58}$, respectively (Fig. 3F). Furthermore, the N-terminal peptide residues play an important role in the natural selectivity of Y_1R against PP. While Y_1R tolerates exchanges in the C-terminal part of NPY to the corresponding PP residues (mainly Q34P, see below), contributions of

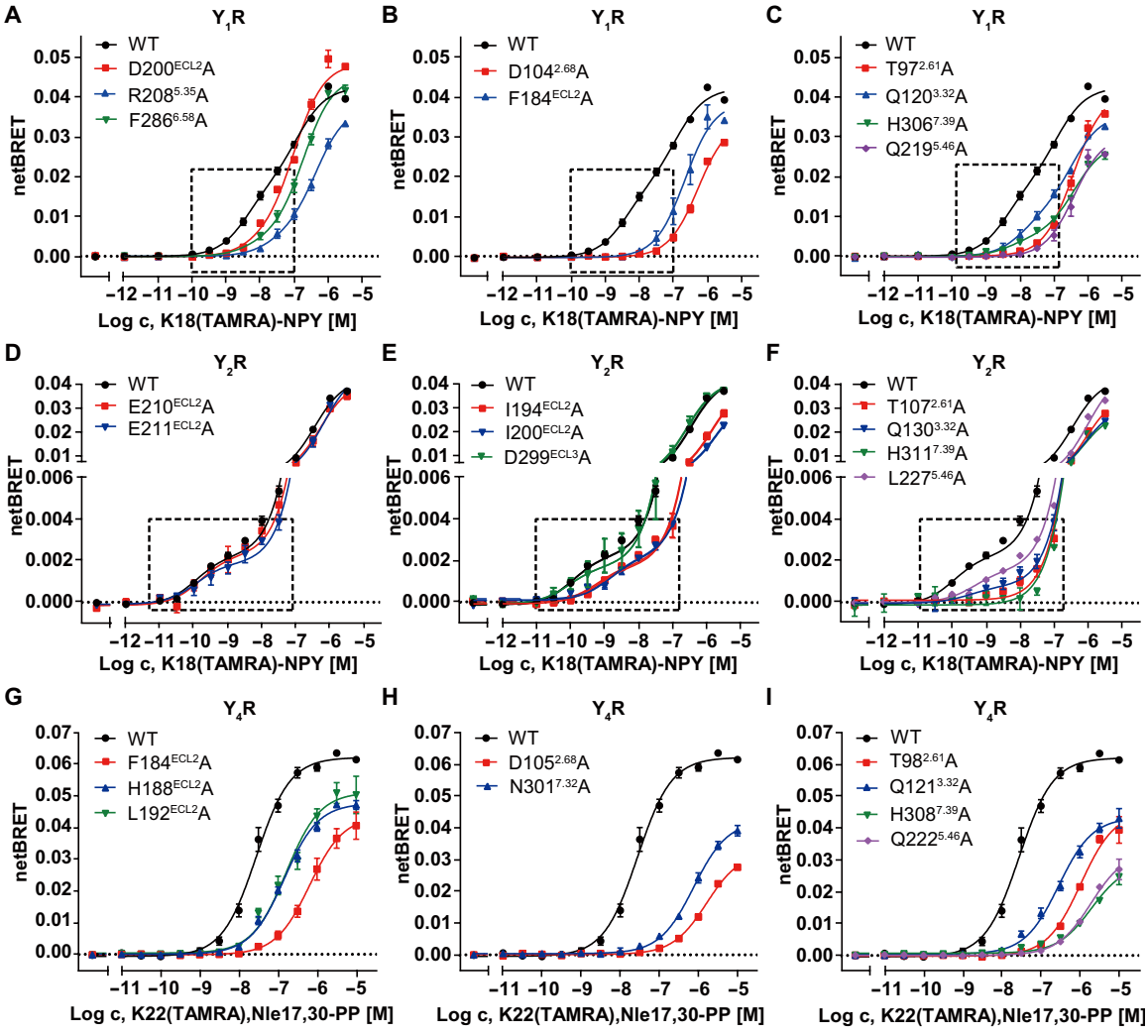

Fig. 4. NanoBRET binding assays of YRs. (**A** to **C**) NanoBRET binding assay measuring K18(TAMRA)-NPY binding to Nluc-Y_1R mutants in isolated cellular membranes. The G protein–stabilized high-affinity state is indicated by a dashed box and is populated less in the Y_1R mutants. (**D** to **F**) NanoBRET binding assay measuring K18(TAMRA)-NPY binding to Nluc-Y_2R mutants in isolated cellular membranes. The G protein–stabilized high-affinity state is indicated by a dashed box and is populated less in many Y_2R mutants except for E210^{ECL2}A, E211^{ECL2}A, and D299ECL3A. (**G** to **I**) NanoBRET binding assay measuring K22(TAMRA),Nle17,30-PP binding to Nluc-Y_4R mutants in intact cells. Mutant receptors have markedly reduced binding affinities. All NanoBRET data are shown as means ± SEM from at least three independent experiments performed in technical triplicate. Table S4 provides detailed numbers of independent experiments (*n*).

Y1 and K4 of NPY are essential for receptor activation, and the corresponding residues in PP (A1 and E4) are not tolerated. The positively charged residue K4 of NPY is within interaction distance of E182 in ECL2 of Y_1R, while the acidic residue E4 in PP forms salt bridges with H185 and H188 in Y_4R. Swapping E4 of PP with K4 of NPY markedly improved the peptide potency at Y_1R [PP, median effective concentration (EC_{50}) = 96 nM; K4-PP, EC_{50} = 12 nM; table S1]. This is further enhanced when reintroducing the large hydrophobic/aromatic Y1 into PP to enable proper engagement into the binding cavity of Y_1R (Y1,K4-PP, EC_{50} = 3.1 nM, potency comparable to NPY at Y_1R; table S1). These observations further support the receptor-specific binding of the N terminus of the NPY peptide at different YRs and provide insight into key factors that govern the distinct interaction modes in this region.

Extracellular loops of YRs mediate NPY peptide recognition

In the NPY peptide–bound YR structures, the N terminus and extracellular loops of the receptor comprise 40 to 61% of the binding interface for the peptide agonist (Y_1R-NPY: 510 Å^2, 1283 Å^2 in total; Y_2R-NPY: 685 Å^2, 1216 Å^2 in total; Y_4R-PP: 865 Å^2, 1416 Å^2 in total). Among the extracellular loops, ECL2 contributes most of the surface area to peptide binding. In all three structures, the hairpin structure of the receptor ECL2 stands upward, with its residues (P183, F184, Y192, V197, and F199 in Y_1R; I192, I194, F198, I200, and A202 in Y_2R; F184, H188, A191, L192, and T202 in Y_4R) forming a hydrophobic core with a patch consisting of residues L24, Y27, I28, and I/L31 in the α helix of NPY and PP (Fig. 3, G to I), which greatly strengthens the binding between the peptide C-terminal region and the receptor. This agrees with previous NMR and mutagenesis studies,

which suggested that the hydrophobic face of the NPY α helix is tethered to ECL2 of Y_2R through hydrophobic contacts mainly with I194 and I200 (*15*). Furthermore, the hydrophobic contacts of F184 and F199 (Y_1R), I200 and A202 (Y_2R), and F184, H188, and L192 (Y_4R) in ECL2 to the α helix of the NPY peptides proved to be functionally important, being reflected by a 4- to 45-fold reduction of the NPY peptide potency in inducing IP accumulation for the corresponding alanine or tryptophan mutants (Fig. 3, M to O, and table S1). This was further corroborated by a 6- to 25-fold reduced affinity of PP at the Y_4R mutants F184A, H188A, and L192A in the NanoBRET binding assay (Fig. 4G, fig. S6, and table S4). Similarly, high-affinity binding of NPY was not detectable for the Y_1R mutant F184A and severely reduced for the Y_2R mutants I194A and I200A (Fig. 4, B and E; fig. S6; and table S4).

In contrast to the common hydrophobic interaction core formed by the receptor ECL2 and the α helix of the NPY peptide, the peptide residue R25 displays receptor-specific polar interactions with the three receptors (Fig. 3, J to L). In Y_2R, the basic side chain "bends away" from the ligand-binding pocket and forms a salt bridge with the acidic residue D299 in ECL3 (Fig. 3K), whereas this interaction is not possible in the Y_1R and Y_4R complexes because of the substitutions by noncharged residues at this position in ECL3 of these receptors. Instead, the side chain of R25 shifts toward the N terminus and ECL1 and is within interaction distance of E29, D32, and $D104^{2.68}$ in Y_1R and D36 and $D105^{2.68}$ in Y_4R, respectively (Fig. 3, J and L). The peptide residue R25 does not contribute much to receptor activation at any of the three receptors (*39*), although peptides carrying an R25A mutation have a moderately decreased binding affinity (*5*) supporting these contacts. Similarly, its counterpart D299 in Y_2R can be mutated to alanine without measurable loss of function (Figs. 3N and 4E and tables S1 and S4). However, in Y_1R and Y_4R, the residue $D^{2.68}$ in the junction between helix II and ECL1 was suggested to be important for NPY and PYY binding by previous mutagenesis studies (*35*, *40*). The importance of this acidic residue for receptor activation was further confirmed in the present study, demonstrating that the mutation $D^{2.68}A$ reduced the agonistic activity of the NPY peptides in inducing IP production at Y_1R and Y_4R by 22- and 538-fold, respectively (Fig. 3, M and O, and table S1), and resulted in a complete loss of the high-affinity binding state of NPY at Y_1R and PP at Y_4R (Fig. 4, B and H; fig. S6; and table S4). In contrast, the corresponding residue in Y_2R, $G114^{2.68}$, precludes this ionic interaction with the peptide.

In addition to stabilizing the high-affinity peptide binding, the receptor extracellular region may also have a role in mediating initial receptor-peptide recognition. This hypothesis is supported by an estimated four- to sixfold decrease in affinity for the low-affinity binding of NPY to the Y_2R mutants I194A and I200A in the NanoBRET assay (wild type, $K_{D,2}$ = 349 nM; I194A and I200A, $K_{D,2} \geq 1$ μM; Fig. 4E), which was the strongest effect on the low-affinity state among all tested positions of Y_2R. At Y_1R, we observed an estimated fourfold reduced affinity in the low-affinity state for the alanine replacement of the residue $D104^{2.68}A$ (wild type, $K_{D,2}$ = 126 nM; $D104^{2.68}A$, $K_{D,2} \geq 500$ nM; Fig. 4B). Furthermore, previous complementary mutagenesis studies of Y_1R demonstrated direct contacts between L30 of NPY and I293 in ECL3 of the receptor and between the NPY residue R33 and $N299^{7.32}$ in the extracellular tip of helix VII (*16*). Similarly, in Y_4R, the residue $N301^{7.32}$ has also been suggested to interact with R33 of PP (*41*). These interactions do not engage in the structurally observed, "final" high-affinity binding pose, but likely mediate the initial recognition process.

Receptor-specific recognition of the peptide C terminus

The pentapeptide T32-Y36 at the C terminus of NPY has been found to be of major importance for binding to all NPY receptors (*2*, *5*). This fragment locates at the bottom of the ligand-binding pocket in the NPY peptide–bound YR structures, inserting into a narrow cavity shaped by helices II to VII (fig. S7B). Comparison with our recently determined structures of antagonist-bound Y_1R (*16*) and Y_2R (*19*) reveals overlapping binding sites for the peptide agonist and small-molecule antagonists. The side chains of R35 and Y36 in NPY overlay well with the argininamide side chain and the hydroxyphenyl group of the Y_1R antagonist UR-MK299, while the NPY residue R33 occupies a binding site similar to that of the diphenylacetyl moiety in the antagonist (fig. S7C). In contrast to the largely overlapping binding sites of the NPY C terminus and UR-MK299, the Y_2R antagonist JNJ-31020028 only partially shares the binding site with NPY, with its fluorophenyl and piperazine groups overlaying with the C-terminal residue Y36 of the agonist (fig. S7D).

The positioning of the C-terminal residues R35-Y36-amide in NPY and PP is remarkably similar in all of the three structures (fig. S7B), which suggests a common mode for receptor activation by the crucial amidated residue Y36 sitting at the bottom of the ligand-binding pocket (Fig. 5, A to C). In all of the three NPY/PP-bound YR structures, a polar interaction network between the amide group of the NPY peptide and three receptor residues $T^{2.61}$, $Q^{3.32}$, and $H^{7.39}$ was identified (Fig. 5, A to C). These three residues are highly conserved in all NPY receptors throughout evolution (*42*, *43*), suggesting that they may have similar key functions in all NPY receptor subtypes. Previous characterization of modifications of the amide group at the peptide C terminus showed a marked loss of binding affinity to Y_1R, Y_2R, and Y_4R (*38*, *44*, *45*), underlining a crucial role of the amide in binding to the NPY receptors. There is only weak agonistic activity for the analog NPY-tyramide lacking the C-terminal amide at Y_1R (*45*) and Y_2R (*15*), implying that breaking the hydrogen-bond network between the peptide agonist and the three polar residues may preclude the conformational changes of the receptor required for receptor activation. Consistent with this finding, the mutations $T^{2.61}A$, $Q^{3.32}A$, and $H^{7.39}A$ in Y_1R, Y_2R, and Y_4R markedly impaired the NPY/PP-induced receptor signaling (6- to 404-fold reduction of EC_{50}), except for $H306^{7.39}A$ of Y_1R (Fig. 5, J to L, and table S1). In the NanoBRET assay, these mutations substantially impaired the high-affinity binding of NPY/PP to the three NPY receptors (Fig. 4, C, F, and I; fig. S6; and table S4), suggesting a reduction of the agonist binding affinity and/or a destabilization of the ternary complex, both of which result in limited signaling. Although the Y_1R mutation $H306^{7.39}A$ had no influence on signal transduction, the binding curve for this mutant shows a changed binding behavior of the peptide agonist, since the BRET window is reduced in both the high- and low-affinity states compared to the wild-type Y_1R. This suggests a change in the binding orientation of the ligand as well as a destabilization of the G protein interaction. However, the complex is still stable enough to induce the maximal G protein activation in our assay setup. Nonetheless, the changes in the BRET signal demonstrate that this position influences binding of NPY to Y_1R.

The bulky side chain of Y36 lies in a subpocket bordered by helices III to VI of the receptor (Fig. 5, A to C), directing its hydroxyl group toward helix V. In the NPY-Y_1R-G_{i1} and PP-Y_4R-G_{i1} complexes, the side-chain hydroxyl moiety is engaged in a hydrogen bond with the receptor residue $Q^{5.46}$ at the bottom of this subpocket (Fig. 5, A and C). The importance of this interaction in mediating

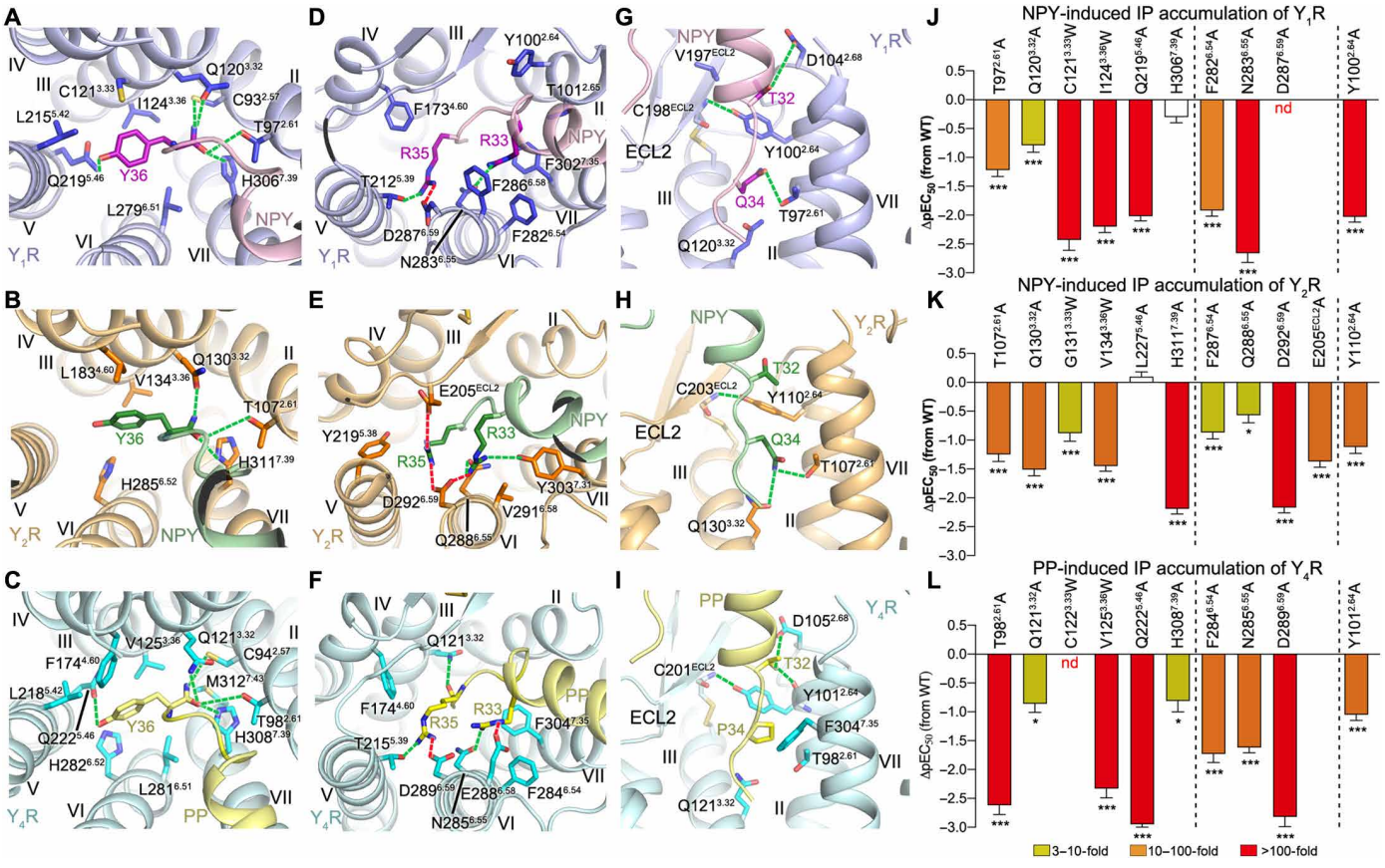

Fig. 5. Receptor-specific interactions between YR and the C terminus of the NPY peptide. (**A** to **C**) Interactions between YR and the peptide residue Y36. (**D** to **F**) Interactions between YR and the peptide residues R33 and R35. (**G** to **I**) Interactions between YR and the peptide residues T32 and Q/P34. The salt bridges and hydrogen bonds are displayed as red and green dashed lines, respectively. (A, D, and G) NPY-Y_1R-G_{i1}; (B, E, and H) NPY-Y_2R-G_{i1}; (C, F, and I) PP-Y_4R-G_{i1}. (**J** to **L**) NPY/PP-induced IP accumulation of YRs. (J) Y_1R mutants; (K) Y_2R mutants; (L) Y_4R mutants. Bars represent differences in calculated peptide potency (pEC_{50}) for each mutant relative to the WT receptor. Data are means ± SEM from at least three independent experiments performed in technical triplicate. *$P < 0.01$; ***$P < 0.0001$ by one-way analysis of variance followed by Dunnett's post-test, compared with the response of the WT receptor. See table S1 for detailed statistical evaluation and expression level. The mutants are divided into three groups using two dashed lines: left, mutants for the residues that interact with Y36 of NPY/PP; middle, mutants for the residues that interact with R33 and R35 of NPY/PP; right, mutant for the residue $Y^{2.64}$ that interacts with T32 of NPY/PP.

Y_1R-agonist binding is supported by previous mutagenesis studies, in which removal of the hydroxyl group of Y36 reduced the binding affinity by 13-fold (*25*) and the mutation $Q219^{5.46}$A in Y_1R abolished peptide agonist binding (*35*). However, this hydrogen-bond interaction does not exist in the NPY-Y_2R-G_{i1} complex because of the hydrophobic replacement $L227^{5.46}$ in Y_2R. This difference in binding mode is consistent with the previous investigation of modifications of Y36, where replacing the side-chain hydroxyl group with electron-withdrawing substituents, which cannot participate in hydrogen bonding, greatly decreased agonist binding to Y_1R and Y_4R but had no effect on Y_2R (*46*). Furthermore, it was observed in our mutagenesis studies that the alanine substitution at position 5.46 reduced the NPY/pp potency in triggering IP production at Y_1R and Y_4R by 107-fold and 861-fold, respectively (Fig. 5, J and L, and table S1). This was further underlined by NanoBRET binding data that exhibit a similar trend, with the Y_1R mutant $Q219^{5.46}$A being devoid of a detectable high-affinity binding state and the corresponding Y_4R mutant displaying an about 100-fold reduction of affinity (Fig. 4, C and I; fig. S6; and table S4). In contrast, the mutation $L227^{5.46}$A in Y_2R showed a more limited effect on receptor function, with a 50% decreased $BRET_{max}$ of the high-affinity binding (Fig. 4F, fig. S6, and table S4), yet an unchanged potency of NPY in inducing IP accumulation (Fig. 5K and table S1).

It has been found that size, position, and orientation of the side chain of Y36 are critical for binding to Y_1R and Y_4R, whereas Y_2R was more tolerant for large size and conformational changes of the side chain (*5*, *46*). These results suggest steric limitations of the binding site for Y36 in Y_1R and Y_4R. The three NPY/PP-YR-G_{i1} structures reveal a narrower binding cavity for Y36 in Y_1R and Y_4R than in Y_2R, owing to the replacements of the Y_2R residues $G^{3.33}$, $L^{4.60}$, $S^{5.42}$, and $L^{5.46}$ with bulkier residues in Y_1R and Y_4R, $C^{3.33}$, $F^{4.60}$, $L^{5.42}$, and $Q^{5.46}$ (fig. S7, E to G). Further reduction of the size of the binding pocket in Y_1R and Y_4R caused by introducing a tryptophan mutation $C^{3.33}$W or $I/V^{3.36}$W led to an over 163-fold reduction of the NPY/PP potency in the IP accumulation assay (Fig. 5, J and L, and table S1). In contrast, the Y_2R mutations $G131^{3.33}$W and $V134^{3.36}$W had a weaker effect on receptor signaling (8- to 28-fold reduction of EC_{50}; Fig. 5K and table S1).

A previous alanine scan of NPY identified that two peptide residues R33 and R35 are the most important residues for Y_1R, Y_2R, and Y_4R binding, with their alanine substitutions associated with an over 170-fold decrease of binding affinity (*5*). Further complementary

mutagenesis studies suggested subtype-specific interactions between these two basic residues and $D^{6.59}$, a conserved NPY receptor residue that has been confirmed to be critical for all subtypes binding to the NPY peptides (*39*) and displayed the most detrimental effect on receptor signaling among all mutants tested in the present study (Fig. 5, J to L, and table S1). It has been proposed that R35 interacts with $D^{6.59}$ in Y_1R and Y_4R, while R33 is the binding partner of $D^{6.59}$ in Y_2R and Y_5R (*39*). In the NPY peptide–bound YR structures, R33 and R35 form multiple polar and hydrophobic interactions with the receptor, but the interaction pattern varies between subtypes (Fig. 5, D to F).

In all the three structures, the peptide residue R35 is located at a very similar position between helices III and VI and forms a salt bridge with $D^{6.59}$ (Fig. 5, D to F). In Y_2R, R35 makes an additional ionic interaction with E205 in ECL2 on the other side of the binding pocket (Fig. 5E). In contrast, R33 forms an ionic contact with $D^{6.59}$ only in Y_2R, while it is oriented more toward $N^{6.55}$ and $F^{6.54}$ in Y_1R and Y_4R, underlined by a marked loss of NPY/PP potency for the corresponding alanine mutants (Fig. 5, J and L, and table S1). This difference is likely due to a spatial hindrance caused by the bulky Y_1R residue $F286^{6.58}$ ($V291^{6.58}$ in Y_2R), which blocks the interaction between R33 and $D^{6.59}$ in the Y_1R-NPY complex (Fig. 5D). In Y_4R, the corresponding residue $E288^{6.58}$ also plays a role in hampering the contact of the PP residue R33 with $D^{6.59}$ by constraining the conformation of the basic peptide residue through a salt bridge (Fig. 5F). The interaction patterns between $D^{6.59}$ and the peptide residues R33 and R35 observed in the NPY/PP-YR-G_{i1} structures agree with the previously proposed subtype-specific interactions (*39*, *44*) except for the additional salt bridge between R35 and $D^{6.59}$ in Y_2R. The double salt bridges of R35 with $D^{6.59}$ and E205 in Y_2R are supported by previous mutagenesis studies showing a notable drop of NPY binding for the Y_2R mutant E205A (*39*, *47*) and the present study, where the mutation E205A was associated with a 23-fold drop of the NPY activity in triggering receptor signaling (Fig. 5K and table S1). Residue $N/Q^{6.55}$ appears to be another key residue for recognition of the NPY peptides, in particular for R33 (Fig. 5, D to F), highlighted by a marked decrease of potency of the NPY peptides for the $N/Q^{6.55}A$ mutants of Y_1R, Y_2R, and Y_4R (Fig. 5, J to L, and table S1). This residue has also been previously identified as a key residue for small-molecule antagonist binding, serving as an important polar anchor (*16*, *35*).

The residue T32 at the C-terminal region of NPY/PP has also proved important for binding to the NPY receptors. This is underlined by the loss of binding affinity of the NPY mutant T32A at Y_1R, Y_2R, and Y_4R (*5*, *25*). This residue is located at the position where the C-terminal pentapeptide unwinds from the regular α helix (fig. S7B). In all the three NPY peptide–bound YR structures, T32 in NPY and PP forms a contact with the receptor residue $Y^{2.64}$ (Fig. 5, G to I). This residue is conserved in the human Y_1R, Y_2R, and Y_4R, but not in Y_5R. While $Y^{2.64}$ does not seem to make specific side-chain polar contacts with NPY or PP at any of the three receptors, its side chain closes off this subpocket toward helix III and its hydroxyl group forms a hydrogen bond with the main chain of the conserved cysteine residue in ECL2, thus stabilizing the fold in the extracellular region (Fig. 5, G to I). Consistent with this structural feature, $Y^{2.64}$ appeared to be critical for peptide agonist binding to both Y_1R and Y_2R in several studies (*35*, *36*, *47*). In addition, the $Y^{2.64}A$ mutation substantially reduced the NPY/PP potency in triggering IP production at Y_1R, Y_2R, and Y_4R (Fig. 5, J to L, and table S1).

The residue at position 34 of the NPY peptides is the only residue showing variability in amino acid at the peptide C terminus (Q34 in NPY and PYY, and P34 in PP; fig. S3L) and has been proposed as a key determinant introducing Y_4R selectivity to PP over NPY and PYY (*2*). Previous mutagenesis studies displayed a distinct behavior of the Q34P-substituted analog of NPY upon binding to different YRs, which retained wild-type affinity at Y_1R and improved binding to Y_4R (*2*), but was not tolerated by Y_2R (*5*), suggesting a diverse binding environment in this region of different receptors. However, the binding site for this peptide residue is largely conserved in these three YRs, and only subtle changes direct the binding specificity. Owing to the close contacts of the α helix of NPY with ECL2 in Y_2R and the interaction of R33 with $D^{6.59}$, the Cα of Q34 is shifted toward the extracellular surface compared to that of NPY bound to Y_1R (fig. S7B). This enables the Q34 side chain to extend into the binding pocket and make a polar interaction with the side chain of $Q^{3.32}$ in Y_2R (Fig. 5H). In contrast, the Cα position of Q34 deeper in the ligand-binding cavity of Y_1R requires the side chain to "bend away" from $Q^{3.32}$ to avoid a steric clash, thus precluding productive polar contacts (Fig. 5G). The Cα of P34 in PP is in an intermediate position at Y_4R compared to that at Y_1R and Y_2R (fig. S7B). While the proline side chain also cannot form polar contacts to $Q^{3.32}$, it packs against helices II and VII stabilizing the rather stretched local conformation of the C terminus of PP (Fig. 5I). Accordingly, the exchange of Q34 in NPY by proline relieves the steric issue in the Y_1R binding pocket and mimics the positioning of PP at Y_4R, resulting in unchanged binding affinity (*5*, *12*). The Q34G variant of NPY is also tolerated at Y_1R but lacks the hydrophobic bulk packing against helices II and VII and may also enhance the local flexibility, explaining the 15-fold loss of binding affinity compared to NPY at Y_1R (*12*). The position 34 is also critical for the natural selectivity of Y_2R against PP. The exchange of Q34 by proline in PP leads to much less favorable binding interactions in the transmembrane pocket compared to NPY at Y_2R. Reversing the corresponding residue in PP to the residue of NPY, however, enables potent interactions of the resulting chimeric peptide with Y_2R: Q34-PP is equipotent with NPY in activating this receptor (*48*). In summary, this work provides detailed molecular maps of the NPY peptides binding to different NPY receptors through subtype-specific interaction patterns, which considerably extend our knowledge about ligand recognition and signal transduction of the NPY-YR system and lay a solid foundation for the development of drugs targeting this physiologically important GPCR family.

MATERIALS AND METHODS

Cloning and expression of YRs and G_{i1}

The human Y_1R, Y_2R, and Y_4R genes were cloned into a modified pFastBac1 vector (Invitrogen) with a HA signal peptide and a Flag tag at the N terminus, and a PreScission protease site followed by a twin-strep-tag (WSHPQFEK-GGGSGGGSGGSA-WSHPQFEK) at the C terminus. To improve protein yield, the C termini of Y_1R, Y_2R, and Y_4R were truncated after F340, V353, and Q342, respectively, using standard QuikChange polymerase chain reaction (PCR). The dominant-negative human $G\alpha_{i1}$ ($DNG\alpha_{i1}$) was generated as previously described (*20*) by introducing four mutations, S47N, G203A, A326S, and E245A (for Y_1R and Y_2R), or five mutations, S47C, G202T, G203A, A326S, and E245A (for Y_4R), to increase stability of the G_i heterotrimer. $DNG\alpha_{i1}$ was also cloned into the modified

pFastBac1 vector. The human $G\beta_1$ and $G\gamma_2$ were cloned into a pFastBac Dual vector (Invitrogen). Coexpression of the receptor (Y_1R, Y_2R, or Y_4R), $DNG\alpha_{i1}$, and $G\beta_1\gamma_2$ was conducted in HighFive insect cells (Invitrogen) using the Bac-to-Bac Expression System (Invitrogen). The HighFive insect cells were cultured in ESF 921 serum-free medium (Expression Systems) at 27°C to a density of 1.5×10^6 cells/ml and then coinfected with high-titer recombinant baculovirus (>10^8 viral particles per ml) of Y_1R (or Y_4R), $DNG\alpha_{i1}$, and $G\beta_1\gamma_2$ at a multiplicity of infection (MOI) of 2:1:1, or Y_2R, $DNG\alpha_{i1}$, and $G\beta_1\gamma_2$ at an MOI of 1:1:1. The cell pellets were collected by centrifugation 48 hours after transfection and stored at −80°C until use.

Cloning, expression, and purification of scFv16

The gene of scFv16 was cloned into the modified pFastBac1 vector with a GP67 secretion signal peptide inserted to the N terminus and a PreScission protease site followed by an 8×His tag attached to the C terminus. The protein was expressed using the HighFive insect cells and was purified as previously described (*22*). The culture supernatant was pH-balanced (20 mM tris-HCl, pH 8.0) and treated with 1 mM $NiCl_2$ and 5 mM $CaCl_2$ at room temperature for 1 hour. Precipitates were then removed by centrifugation at 160,000*g* for 30 min. The supernatant was incubated with Ni-NTA Superflow resin (Qiagen) in the presence of 5 mM imidazole at 4°C for 2 hours. The resin was washed with 20 column volumes of buffer A [20 mM Hepes (pH 7.5), 500 mM NaCl, and 10 mM imidazole] and 20 column volumes of buffer B [20 mM Hepes (pH 7.5), 100 mM NaCl, and 10 mM imidazole]. The protein was then eluted with 10 column volumes of buffer B supplemented with 250 mM imidazole and flowed through a PD MiniTrap G-25 column (GE Healthcare) to remove the imidazole. After treatment with the His-tagged PreScission protease (custom-made) at 4°C overnight, the protein sample was incubated with Ni-NTA Superflow resin at 4°C for 1 hour to remove the cleaved C-terminal His tag and PreScission protease. The protein was further purified by size exclusion chromatography using a Superdex 75 10/300 GL column (GE Healthcare) to collect monomeric fractions of scFv16, and then the protein was concentrated to 1 to 2 mg ml^{-1} and stored at −80°C until use.

Purification of NPY/PP-YR-G_{i1} complexes

The cell pellets of Y_1R-G_{i1}, Y_2R-G_{i1}, or Y_4R-G_{i1} were thawed on ice and then suspended in a buffer containing 20 mM Hepes (pH 7.5), 100 mM NaCl, 10% (v/v) glycerol, 10 mM $MgCl_2$, and protease inhibitors [4-(2-aminoethyl)benzenesulfonyl fluoride hydrochloride (AEBSF) (10 μg ml^{-1}), E64 (50 μg ml^{-1}), aprotinin (50 μg ml^{-1}), and leupeptin (50 μg ml^{-1})] using a dounce homogenizer. To enable NPY-YR-G_{i1} complex formation, the cell suspension was supplemented with 25 μM NPY peptide (human NPY for Y_1R and Y_2R; human PP for Y_4R), scFv16 (30 to 50 μg ml^{-1}) (only for Y_1R and Y_2R), 100 μM tris(2-chloroethyl)phosphate (TCEP), and apyrase (50 mU ml^{-1}) (NEB) and incubated at room temperature for 1.5 hours. The NPY-Y_1R-G_{i1}-scFv16 complex was then extracted from the cell membranes by adding 0.5% (w/v) lauryl maltose neopentyl glycol (LMNG; Anatrace) and 0.05% (w/v) cholesterol hemisuccinate (CHS; Sigma-Aldrich), while the cells of the NPY-Y_2R-G_{i1}-scFv16 or PP-Y_4R-G_{i1} complex were solubilized with addition of 0.027% glyco-diosgenin (GDN; Anatrace). The mixtures were further supplemented with NPY (for Y_1R and Y_2R) or PP (for Y_4R) to the final concentration of 50 μM and incubated at 4°C for 2 hours. The solubilized samples were collected by centrifugation at 160,000*g* for 30 min and incubated with Strep-Tactin XT Superflow resin (IBA Lifesciences) at 4°C overnight.

For the NPY-Y_1R-G_{i1}-scFv16 complex, the strep resin was washed with a buffer containing 20 mM Hepes (pH 7.5), 100 mM NaCl, 10 mM $MgCl_2$, 10% (v/v) glycerol, 0.004% (w/v) LMNG, 0.0004% (w/v) CHS, and 25 μM NPY, and then eluted with a buffer containing 150 mM tris-HCl (pH 8.0), 150 mM NaCl, 10 mM $MgCl_2$, 10% (v/v) glycerol, 0.004% (w/v) LMNG, 0.0004% (w/v) CHS, 25 μM NPY, and 50 mM biotin (Sigma-Aldrich). The NPY-Y_2R-G_{i1}-scFv16 and PP-Y_4R-G_{i1} complexes were purified in the same buffers with addition of 0.0033% GDN, and PP was used instead of NPY for the Y_4R complex. The eluates were further purified by size exclusion chromatography using a Superdex 200 Increase 10/300 GL column (GE Healthcare). The fractions of the NPY-Y_1R-G_{i1}-scFv16 complex were collected in a buffer of 20 mM Hepes (pH 7.5), 100 mM NaCl, 2 mM $MgCl_2$, 0.001% (w/v) LMNG, 0.0001% (w/v) CHS, and 5 μM NPY, while the NPY-Y_2R-G_{i1}-scFv16 and PP-Y_4R-G_{i1} complexes were pooled in a similar buffer containing 20 mM Hepes (pH 7.5), 100 mM NaCl, 2 mM $MgCl_2$, 0.00075% (w/v) LMNG, 0.00025% (w/v) GDN, 0.000075% (w/v) CHS, and 5 μM NPY/PP. The purified NPY-Y_1R-G_{i1}-scFv16, NPY-Y_2R-G_{i1}-scFv16, and PP-Y_4R-G_{i1} complexes were concentrated to 1.5, 1.0, and 0.7 mg ml^{-1}, respectively, with a 100-kDa molecular weight cutoff concentrator (Sartorius Stedim Biotech).

Cryo-EM data acquisition

The grids of the NPY/PP-YR-G_{i1} complexes were made by applying 3-μl protein samples onto the glow-discharged holey carbon grids (Quantifoil R0.6/1, Au 300 mesh for the Y_1R and Y_2R complexes; CryoMatrix R1.2/1.3, Au 300 mesh for the Y_4R complex). The grids were then blotted with a blot time of 2 s (Y_1R and Y_2R) or 1 s (Y_4R) and blot force of 0 at 4°C under 100% humidity and plunge-frozen in liquid ethane using Vitrobot Mark IV (Thermo Fisher Scientific).

Imaging of the NPY-Y_1R-G_{i1}-scFv16 complex was performed on a Titan Krios G3 electron microscope (FEI) equipped with a K3 Summit direct electron detector (Gatan) at 300 kV. The GIF-Quantum energy filter was set to zero loss mode with slit width of 20 eV to eliminate inelasticity scattering. SerialEM (*49*) program was used to collect data automatically in the super-resolution counting mode with a pixel size of 1.045. A total of 12,489 movie stacks were acquired with the defocus values ranging from −1.3 to −2.3 μm and a dose rate of 2.1875 electrons per $Å^2$ per frame. Each movie stack was generated by 3-s exposure with 32 frames.

For the NPY-Y_2R-G_{i1}-scFv16 complex, the imaging was conducted on a 300-kV Titan Krios electron microscope (FEI) equipped with a K2 Summit direct electron detector (Gatan). Using the SerialEM program, a total of 8966 movie stacks were automatically recorded in a pixel size of 0.82, with the defocus values ranging from −1.3 to −2.3 μm, and exposed to a dose rate of 1.875 electrons per $Å^2$ per frame. Each movie stack contains 32 frames for a total dose of 60 electrons per $Å^2$.

For the PP-Y_4R-G_{i1} complex, the imaging was performed on a Titan Krios G3 electron microscope (FEI) equipped with a K3 Summit direct electron detector (Gatan) and a GIF-Quantum energy filter at 300 kV. A total of 9754 movie stacks were collected automatically in a pixel size of 1.045 using the SerialEM program. The defocus values ranged from −0.8 to −1.5 μm, and the dose rate is 1.75 electrons per $Å^2$ per frame. Each movie stack contains 40 frames for a total dose of 70 electrons per $Å^2$.

Cryo-EM data processing

All cryo-EM data were processed with RELION-3 (*50*) and cryoSPARC (*51*). MotionCor2 (*52*) was used to correct the drift and beam-induced motion. The contrast transfer function (CTF) for each micrograph was estimated by using Gctf (*53*). Gautomatch (developed by K. Zhang, MRC Laboratory of Molecular Biology, Cambridge, UK; https://www2.mrc-lmb.cam.ac.uk/download/gautomatch-056/) was used to autopick and extract particle projections for initial 2D classification, 3D classification, and initial refinement on RELION-3.0. After discarding false-positive particles, 11,739,454 NPY-Y_1R-G_{i1}-scFv16 particles, 2,822,634 NPY-Y_2R-G_{i1}-scFv16 particles, and 6,297,193 PP-Y_4R-G_{i1} particles were used for further data processing (see fig. S1, C, I, and O for details). The final maps were improved by Bayesian polishing, resulting in a 3.2-Å map of NPY-Y_1R-G_{i1}-scFv16 using 423,400 particles, a 3.44-Å map of NPY-Y_2R-G_{i1}-scFv16 with 361,477 particles, and a 3.0-Å map of PP-Y_4R-G_{i1} using 1,047,385 particles. The scFv16 portion with unambiguous map densities was masked in both the Y_1R and Y_2R complex structures. The local resolution for the maps was generated by ResMap (*54*). The 3D variability analysis was performed in CryoSPARC.

Model building

The model building of the NPY-Y_1R-G_{i1} and NPY-Y_2R-G_{i1} complexes was started by using the receptor portion in the crystal structure of Y_1R–UR-MK299 [Protein Data Bank (PDB) code: 5ZBQ] or Y_2R–JNJ-31020028 (PDB code: 7DDZ), the G protein subunits ($G\alpha_{i1}$, $G\beta_1$, and $G\gamma_2$) in the cryo-EM structure of G_i-bound CB1 (PDB code: 6N4B), and the NMR structure of NPY (PDB code: 1RON) as initial models. For the PP-Y_4R-G_{i1} complex, a Y_4R model was generated using the SWISS-MODEL workspace (*55*) with the Y_1R–BMS-193885 structure (PDB code: 5ZBH) as the initial model. The Y_4R model, together with the G protein in the CB1-G_{i1} complex and the NMR structure of PP (PDB code: 1BBA), was then applied to build the Y_4R complex model. The UCSF Chimera (*56*) was used to dock the initial models individually into the electron density maps. The three starting models were iteratively manually adjusted in COOT (*57*) and automatically refined by phenix.real_space_refine in Phenix (*58*). The final models were validated by MolProbity (*59*), and the refinement statistics are provided in table S2. All structure figures were prepared using PyMOL (https://pymol.org/2/).

IP accumulation assay

The N-terminal flag-tagged wild-type receptor, receptor mutants, and a chimeric G protein $G\alpha_{\Delta 6qi4myr}$, which redirects the $G\alpha_i$ signaling pathway to the $G\alpha_q$ phospholipase C pathway (*60*), were cloned into the expression vector pcDNA3.1/V5-His-TOPO (Invitrogen). The human embryonic kidney (HEK) 293F cells (Invitrogen) were cultured in Dulbecco's modified Eagle's medium (DMEM; Gibco) to a density of about 1.2×10^6 cells/ml at 37°C and cotransfected with the plasmid of the wild type or mutants together with the $G\alpha_{\Delta 6qi4myr}$ plasmid at the ratio of 4:1 (w/w, 8 μg:2 μg in 10 ml of HEK293F cells) using PEI-MAXI 4000 (Polysciences) transfection protocol. The transfected cells were cultured at 37°C for 48 hours. The cell surface expression level was detected by incubating 10 μl of cells with 10 μl of monoclonal anti-FLAG M2–fluorescein isothiocyanate antibody (Sigma-Aldrich) diluted by tris-buffered saline (v/v, 1:10) and supplemented with 4% (w/w) bovine serum albumin (BSA) at 4°C for 20 min in the dark. The fluorescent signal of the bound antibody was measured using an FCM (Flow Cytometry) reader (Millipore).

An HRRF IP-One Gq kit (CisBio Bioassays) was used to conduct the IP accumulation assay. The cell pellets were collected by centrifugation at 150*g* for 3 min, resuspended in a stimulation buffer, and added into 384-well plates (10,000, 20,000, and 20,000 cells per well for Y_1R, Y_2R, and Y_4R, respectively). The cells expressing Y_1R and Y_2R were incubated with increased concentrations of NPY (1 pM to 10 μM) at 37°C for 1.5 hours, while the Y_4R cells were treated with 1 pM to 10 μM PP at 37°C for 2 hours. The dye d2-labeled IP1 and the terbium cryptate–labeled anti-IP1 monoclonal antibody were diluted in Lysis Buffer (1:20) and added into the wells for 1-hour incubation at room temperature. The fluorescent signal was measured by a microplate reader (Synergy H1) with excitation at 330 nm and emission at 620 and 665 nm. GraphPad Prism 8.0 (GraphPad Software) was used to plot the concentration-response curves. The accumulation of IP1 was calculated according to a standard concentration-response curve.

NanoBRET ligand-binding assay

To characterize ligand binding to Y_1R, Y_2R, Y_4R, and corresponding mutants generated by standard QuikChange or Q5 (NEB) PCR, a NanoBRET-based binding assay was performed. A small nanoluciferase (Nluc) (*61*) is genetically fused to the N termini of the receptors and functions as a donor for BRET to a tetramethylrhodamine (TAMRA) fluorophore–labeled analog of NPY or PP (acceptor). The fluorophore was labeled at residue K18 replacing the endogenous A18, as this position remains solvent-exposed when NPY is bound to Y_1R and Y_2R and corresponding mutants. For PP, position K22 was labeled with TAMRA and the residues M17 and M30 were substituted with norleucine (Nle). Membrane localization of Y_1R, Y_2R, Y_4R, and corresponding mutants was analyzed independently using fluorescence microscopy using a C-terminal eYFP fusion protein as described previously (*19*). Briefly, HEK293 cells were grown to 70% confluency in eight-well μ-slides (IBIDItreat, Martinsried, Germany) and transiently transfected with 1000 ng of plasmid DNA using Lipofectamine 2000 (Invitrogen, Carlsbad, USA). After 16 to 24 hours, medium was replaced with Opti-MEM (Gibco Thermo Fisher, Waltham, USA) and nuclei were stained with 0.5 ng of Hoechst 33342 nuclear stain (Sigma-Aldrich, St. Louis, USA) for 30 min. Living cells were observed with an Axio Observer Z1 microscope with ApoTome.2 (Zeiss, Oberkochen, Germany; filter 46 excitation 500/20, FT 515, emission 535/30; filter 02 excitation 365, FT 395, emission LP 420).

For the NanoBRET ligand-binding assay, all required buffers and solutions were stored on ice or at 4°C until use. Saturation binding experiments with K18(TAMRA)-NPY and K22(TAMRA),Nle17,30-PP were performed using intact transiently transfected HEK293 cells or membranes prepared thereof as previously described (*19*, *62*) and were conducted in solid black 96-well microplates. Membrane preparations were thawed slowly on ice and resuspended by pipetting up and down several times and diluted in BRET buffer (Hanks' balanced salt solution supplemented with 25 mM Hepes, pH 7.4) supplemented with 0.1% BSA and 50 μM Pefabloc to yield a total luminescence of 500,000 to 1,000,000 relative luminescence units (RLU) (430- to 470-nm bandwidth) per well, which corresponded to 0.25 to 0.7 μg of total protein. The diluted membrane preparations were stored on ice until further use. Coelenterazine H was used as the luciferase substrate for signal detection and was diluted from a 1 μg μl^{-1} (in EtOH, stored at −20°C) stock solution in BRET

buffer to a concentration of 42 μM (10-fold higher than the final concentration) shortly before the BRET measurement.

The fluorescently labeled NPY/PP was serially diluted to a concentration of $10^{-4.5}$ to 10^{-11} M in Milli-Q water supplemented with 0.1% BSA (10-fold higher than the final concentration). Ten microliters of the serially diluted TAMRA-peptide was transferred into a solid black 96-well plate ($10^{-5.5}$ to 10^{-12} M final concentration in an assay volume of 100 μl). For the control not containing any fluorescent peptide (wo), 10 μl of Milli-Q water supplemented with 0.1% BSA was transferred into a well of a solid black 96-well plate. Eighty microliters of the membrane suspension was added to every well (0.25 to 0.7 μg total amount of protein in 100 μl of assay volume). The plates were shaken in the dark at room temperature for 10 min. Then, 10 μl of the coelenterazine H working solution in BRET buffer was added to each well (4.2 μM final concentration in 100 μl of assay volume). Subsequently, the BRET signal was measured at room temperature using a Tecan Spark plate reader (Tecan).

When using intact cells for the binding experiments, cells were transiently transfected in T25 flasks using 1.7 μg of plasmid DNA and 6.4 μl of Metafectene Pro according to the manufacturer's protocol overnight at 37°C. On the next day, 50,000 cells per well were reseeded in black solid-bottom 96-well plates, incubated overnight at 37°C, and used for the binding assay as described, but ligand incubation was carried out on ice to prevent receptor internalization.

The luminescence signal was detected between 430 and 470 nm. The TAMRA fluorescence signal was detected between 550 and 700 nm. BRET was calculated as the ratio of the emission signals from TAMRA fluorescence and luminescence. The netBRET was obtained by baseline correction using the calculated mean value composed of the wo control (without the labeled ligand). The BRET ligand-binding assays were performed in triplicates with at least three independent experiments. Data analysis was undertaken using the software GraphPad Prism 5.0 or 9.0. The obtained netBRET values were plotted against the logarithmically scaled concentrations of K18(TAMRA)-NPY or K22(TAMRA),Nle17,30-PP. To determine $EC_{50\_high\text{-}affinity\ site}$ and $EC_{50\_low\text{-}affinity\ site}$ values, data were analyzed using nonlinear regression and fitting to equation "biphasic." For biphasic fitting, nH1 and nH2 were set to 1.

Cyclic adenosine 3′,5′-monophosphate (cAMP) assay

To measure $G_{i/o}$ activation downstream signaling of wild-type and Nluc-tagged receptors, HEK293 cells were seeded in six-well plates at a density of 1.25×10^6 per well. At a confluency of approximately 70 to 80%, cells were transfected with a total of 4 μg of plasmid DNA using Metafectene Pro (Biontex) according to the manufacturer's protocol. The DNA mixture contained 2 μg of plasmid encoding the receptor and 2 μg of the luciferase reporter plasmid pGL4.29[luc2P/CRE/Hygro] (Promega), which codes for a destabilized version of a *Photinus pyralis* luciferase under the control of a cAMP–response element. Sixteen hours after transfection, cells were reseeded into white 384-well plates at a density of 15,000 cells per well. The next day, medium was discarded and cells were stimulated with 15 μl of the peptide dilution series in serum-free DMEM medium, where forskolin was freshly added to a final concentration of 1 μM to elevate cellular cAMP levels. After 3-hour incubation at 37°C, cells were re-equilibrated to room temperature, 15 μl of OneGlo luciferase substrate in lysis buffer (Promega) was added, and luminescence was measured in a plate reader (Tecan Spark, Tecan).

The assays were performed three times independently in technical triplicate. Data were normalized to buffer/ + 1 μM forskolin-only and buffer (no forskolin)–only treated cells and were analyzed with GraphPad Prism 5.0 using a three-parameter logistic fit with fixed Hill slope of $n_H = 1$.

Radioactive ligand-binding assay

Radioactive ligand-binding assays were performed using membrane preparations of transiently transfected HEK293 cells, prepared as described above for the NanoBRET binding assays, and stored in aliquots at −80°C. Radioligand and unlabeled peptides were diluted in distilled water containing 1% BSA. To determine the K_D values, 10 μl of 10 × concentrated ^{125}I-PYY (NEX240; 81.4 TBq/mmol; PerkinElmer) was added to a 96-well plate (final concentration, 0 to 400 pM), followed by adding 10 μl of 1% BSA solution (total binding) or 10 μl of unlabeled NPY at a concentration of 10 μM (final concentration: 1 μM; unspecific binding), respectively. Eighty microliters of membranes containing 0.5 μg (for Y_2R membranes) or 1.5 μg (for Y_1R membranes) of total protein in a membrane buffer [25 mM Hepes (pH 7.4), 25 mM $CaCl_2$, 1 mM $MgCl_2$, 50 μM Pefabloc, and 1% BSA] was added. The exact concentration of the radioligand was determined by liquid scintillation counting in each experiment.

Samples were incubated under gentle agitation for 3 hours at room temperature and binding assays were terminated by filtration using the MicroBeta Filtermat-96 Cell Harvester System (PerkinElmer). Filtermats were pretreated freshly with 0.1% (w/v) polyethylenimine in Dulbecco's phosphate-buffered saline (PBS) to reduce nonspecific binding. The membranes were washed three times with ~200 μl of ice-cold PBS and air-dried, and the Meltilex solid scintillator (PerkinElmer) was melted onto the membranes. Radioactivity was determined by scintillation counting (MicroBeta2; PerkinElmer). Binding assays were performed three times independently in technical duplicate. Nonspecific binding was subtracted from all data. Nonlinear regression was performed using GraphPad Prism 5.0 using one-site specific binding (K_D).

SUPPLEMENTARY MATERIALS

Supplementary material for this article is available at https://science.org/doi/10.1126/sciadv.abm1232

View/request a protocol for this paper from *Bio-protocol*.

REFERENCES AND NOTES

1. D. Larhammar, Evolution of neuropeptide Y, peptide YY and pancreatic polypeptide. *Regul. Pept.* **62**, 1–11 (1996).
2. X. Pedragosa-Badia, J. Stichel, A. G. Beck-Sickinger, Neuropeptide Y receptors: How to get subtype selectivity. *Front. Endocrinol.* **4**, 5 (2013).
3. M. C. Michel, A. Beck-Sickinger, H. Cox, H. N. Doods, H. Herzog, D. Larhammar, R. Quirion, T. Schwartz, T. Westfall, XVI. International Union of Pharmacology recommendations for the nomenclature of neuropeptide Y, peptide YY, and pancreatic polypeptide receptors. *Pharmacol. Rev.* **50**, 143–150 (1998).
4. D. Larhammar, Structural diversity of receptors for neuropeptide Y, peptide YY and pancreatic polypeptide. *Regul. Pept.* **65**, 165–174 (1996).
5. C. Cabrele, A. G. Beck-Sickinger, Molecular characterization of the ligand-receptor interaction of the neuropeptide Y family. *J. Pept. Sci.* **6**, 97–122 (2000).
6. D. Lindner, J. Stichel, A. G. Beck-Sickinger, Molecular recognition of the NPY hormone family by their receptors. *Nutrition* **24**, 907–917 (2008).
7. A. Lecklin, I. Lundell, S. Salmela, P. T. Männistö, A. G. Beck-Sickinger, D. Larhammar, Agonists for neuropeptide Y receptors Y1 and Y5 stimulate different phases of feeding in guinea pigs. *Br. J. Pharmacol.* **139**, 1433–1440 (2003).
8. R. L. Batterham, M. A. Cowley, C. J. Small, H. Herzog, M. A. Cohen, C. L. Dakin, A. M. Wren, A. E. Brynes, M. J. Low, M. A. Ghatei, R. D. Cone, S. R. Bloom, Gut hormone PYY_{3-36} physiologically inhibits food intake. *Nature* **418**, 650–654 (2002).

9. N. Sato, Y. Ogino, S. Mashiko, M. Ando, Modulation of neuropeptide Y receptors for the treatment of obesity. *Expert Opin. Ther. Pat.* **19**, 1401–1415 (2009).
10. C. Walther, K. Mörl, A. G. Beck-Sickinger, Neuropeptide Y receptors: Ligand binding and trafficking suggest novel approaches in drug development. *J. Pept. Sci.* **17**, 233–246 (2011).
11. E. Yulyaningsih, L. Zhang, H. Herzog, A. Sainsbury, NPY receptors as potential targets for anti-obesity drug development. *Br. J. Pharmacol.* **163**, 1170–1202 (2011).
12. A. Kaiser, L. Wanka, I. Ziffert, A. G. Beck-Sickinger, Biased agonists at the human Y1 receptor lead to prolonged membrane residency and extended receptor G protein interaction. *Cell. Mol. Life Sci.* **77**, 4675–4691 (2020).
13. S. Ostergaard, J. Kofoed, J. F. Paulsson, K. G. Madsen, R. Jorgensen, B. S. Wulff, Design of Y_2 receptor selective and proteolytically stable PYY_{3-36} analogues. *J. Med. Chem.* **61**, 10519–10530 (2018).
14. C. Cabrele, M. Langer, R. Bader, H. A. Wieland, H. N. Doods, O. Zerbe, A. G. Beck-Sickinger, The first selective agonist for the neuropeptide YY_5 receptor increases food intake in rats. *J. Biol. Chem.* **275**, 36043–36048 (2000).
15. A. Kaiser, P. Müller, T. Zellmann, H. A. Scheidt, L. Thomas, M. Bosse, R. Meier, J. Meiler, D. Huster, A. G. Beck-Sickinger, P. Schmidt, Unwinding of the C-terminal residues of neuropeptide Y is critical for Y_2 receptor binding and activation. *Angew. Chem. Int. Ed. Engl.* **54**, 7446–7449 (2015).
16. Z. Yang, S. Han, M. Keller, A. Kaiser, B. J. Bender, M. Bosse, K. Burkert, L. M. Kögler, D. Wifling, G. Bernhardt, N. Plank, T. Littmann, P. Schmidt, C. Yi, B. Li, S. Ye, R. Zhang, B. Xu, D. Larhammar, R. C. Stevens, D. Huster, J. Meiler, Q. Zhao, A. G. Beck-Sickinger, A. Buschauer, B. Wu, Structural basis of ligand binding modes at the neuropeptide Y Y_1 receptor. *Nature* **556**, 520–524 (2018).
17. A. J. Venkatakrishnan, X. Deupi, G. Lebon, C. G. Tate, G. F. Schertler, M. M. Babu, Molecular signatures of G-protein-coupled receptors. *Nature* **494**, 185–194 (2013).
18. J. A. Ballesteros, H. Weinstein, in *Methods in Neurosciences*, S. C. Sealfon, Ed. (Academic Press, 1995), vol. 25, pp. 366–428.
19. T. Tang, C. Hartig, Q. Chen, W. Zhao, A. Kaiser, X. Zhang, H. Zhang, H. Qu, C. Yi, L. Ma, S. Han, Q. Zhao, A. G. Beck-Sickinger, B. Wu, Structural basis for ligand recognition of the neuropeptide Y Y_2 receptor. *Nat. Commun.* **12**, 737 (2021).
20. C. J. Draper-Joyce, M. Khoshouei, D. M. Thal, Y.-L. Liang, A. T. N. Nguyen, S. G. B. Furness, H. Venugopal, J.-A. Baltos, J. M. Plitzko, R. Danev, W. Baumeister, L. T. May, D. Wootten, P. M. Sexton, A. Glukhova, A. Christopoulos, Structure of the adenosine-bound human adenosine A_1 receptor-G_i complex. *Nature* **558**, 559–563 (2018).
21. Y. Kang, O. Kuybeda, P. W. de Waal, S. Mukherjee, N. van Eps, P. Dutka, X. E. Zhou, A. Bartesaghi, S. Erramilli, T. Morizumi, X. Gu, Y. Yin, P. Liu, Y. Jiang, X. Meng, G. Zhao, K. Melcher, O. P. Ernst, A. A. Kossiakoff, S. Subramaniam, H. E. Xu, Cryo-EM structure of human rhodopsin bound to an inhibitory G protein. *Nature* **558**, 553–558 (2018).
22. A. Koehl, H. Hu, S. Maeda, Y. Zhang, Q. Qu, J. M. Paggi, N. R. Latorraca, D. Hilger, R. Dawson, H. Matile, G. F. X. Schertler, S. Granier, W. I. Weis, R. O. Dror, A. Manglik, G. Skiniotis, B. K. Kobilka, Structure of the μ-opioid receptor-G_i protein complex. *Nature* **558**, 547–552 (2018).
23. K. Krishna Kumar, M. Shalev-Benami, M. J. Robertson, H. Hu, S. D. Banister, S. A. Hollingsworth, N. R. Latorraca, H. E. Kato, D. Hilger, S. Maeda, W. I. Weis, D. L. Farrens, R. O. Dror, S. V. Malhotra, B. K. Kobilka, G. Skiniotis, Structure of a signaling cannabinoid receptor 1-G protein complex. *Cell* **176**, 448–458.e12 (2019).
24. H. E. Kato, Y. Zhang, H. Hu, C.-M. Suomivuori, F. M. N. Kadji, J. Aoki, K. Krishna Kumar, R. Fonseca, D. Hilger, W. Huang, N. R. Latorraca, A. Inoue, R. O. Dror, B. K. Kobilka, G. Skiniotis, Conformational transitions of a neurotensin receptor 1-G_{i1} complex. *Nature* **572**, 80–85 (2019).
25. A. G. Beck-Sickinger, H. A. Weland, H. Wittneben, K. D. Willim, K. Rudolf, G. Jung, Complete L-alanine scan of neuropeptide Y reveals ligands binding to Y_1 and Y_2 receptors with distinguished conformations. *Eur. J. Biochem.* **225**, 947–958 (1994).
26. T. L. Blundell, J. E. Pitts, I. J. Tickle, S. P. Wood, C.-W. Wu, X-ray analysis (1.4-Å resolution) of avian pancreatic polypeptide: Small globular protein hormone. *Proc. Natl. Acad. Sci. U.S.A.* **78**, 4175–4179 (1981).
27. R. Bader, A. Bettio, A. G. Beck-Sickinger, O. Zerbe, Structure and dynamics of micelle-bound neuropeptide Y: Comparison with unligated NPY and implications for receptor selection. *J. Mol. Biol.* **305**, 307–329 (2001).
28. S. A. Monks, G. Karagianis, G. J. Howlett, R. S. Norton, Solution structure of human neuropeptide Y. *J. Biomol. NMR* **8**, 379–390 (1996).
29. A. Bettio, V. Gutewort, A. Pöppl, M. C. Dinger, O. Zschörnig, K. Arnold, C. Toniolo, A. G. Beck-Sickinger, Electron paramagnetic resonance backbone dynamics studies on spin-labelled neuropeptide Y analogues. *J. Pept. Sci.* **8**, 671–682 (2002).
30. A. Bettio, M. C. Dinger, A. G. Beck-Sickinger, The neuropeptide Y monomer in solution is not folded in the pancreatic-polypeptide fold. *Protein Sci.* **11**, 1834–1844 (2002).
31. A. G. Beck-Sickinger, G. Jung, Structure-activity relationships of neuropeptide Y analogues with respect to Y_1 and Y_2 receptors. *Biopolymers* **37**, 123–142 (1995).
32. M. Soave, L. A. Stoddart, A. Brown, J. Woolard, S. J. Hill, Use of a new proximity assay (NanoBRET) to investigate the ligand-binding characteristics of three fluorescent ligands to the human β_1-adrenoceptor expressed in HEK-293 cells. *Pharmacol. Res. Perspect.* **4**, e00250 (2016).
33. L. A. Stoddart, L. E. Kilpatrick, S. J. Hill, NanoBRET approaches to study ligand binding to GPCRs and RTKs. *Trends Pharmacol. Sci.* **39**, 136–147 (2018).
34. D. A. Kirby, S. C. Koerber, A. G. Craig, R. D. Feinstein, L. Delmas, M. R. Brown, J. E. Rivier, Defining structural requirements for neuropeptide Y receptors using truncated and conformationally restricted analogues. *J. Med. Chem.* **36**, 385–393 (1993).
35. M. Sautel, K. Rudolf, H. Wittneben, H. Herzog, R. Martinez, M. Munoz, W. Eberlein, W. Engel, P. Walker, A. G. Beck-Sickinger, Neuropeptide Y and the nonpeptide antagonist BIBP 3226 share an overlapping binding site at the human Y_1 receptor. *Mol. Pharmacol.* **50**, 285–292 (1996).
36. P. Sjödin, S. K. S. Holmberg, H. Akerberg, M. M. Berglund, N. Mohell, D. Larhammar, Re-evaluation of receptor-ligand interactions of the human neuropeptide Y receptor Y1: A site-directed mutagenesis study. *Biochem. J.* **393**, 161–169 (2006).
37. T. Kannoa, A. Kanatani, S. L. Keen, S. Arai-Otsuki, Y. Haga, T. Iwama, A. Ishihara, A. Sakuraba, H. Iwaasa, M. Hirose, H. Morishima, T. Fukami, M. Ihara, Different binding sites for the neuropeptide Y Y1 antagonists 1229U91 and J-104870 on human Y1 receptors. *Peptides* **22**, 405–413 (2001).
38. J. A. Bard, M. W. Walker, T. A. Branchek, R. L. Weinshank, Cloning and functional expression of a human Y4 subtype receptor for pancreatic polypeptide, neuropeptide Y, and peptide YY. *J. Biol. Chem.* **270**, 26762–26765 (1995).
39. N. Merten, D. Lindner, N. Rabe, H. Römpler, K. Mörl, T. Schöneberg, A. G. Beck-Sickinger, Receptor subtype-specific docking of $Asp^{6.59}$ with C-terminal arginine residues in Y receptor ligands. *J. Biol. Chem.* **282**, 7543–7551 (2007).
40. P. Du, J. A. Salon, J. A. Tamm, C. Hou, W. Cui, M. W. Walker, N. Adham, D. S. Dhanoa, I. Islam, P. J. Vaysse, B. Dowling, Y. Shifman, N. Boyle, H. Rueger, T. Schmidlin, Y. Yamaguchi, T. A. Branchek, R. L. Weinshank, C. Gluchowski, Modeling the G-protein-coupled neuropeptide Y Y1 receptor agonist and antagonist binding sites. *Protein Eng.* **10**, 109–117 (1997).
41. X. Pedragosa-Badia, G. R. Sliwoski, E. Dong Nguyen, D. Lindner, J. Stichel, K. W. Kaufmann, J. Meiler, A. G. Beck-Sickinger, Pancreatic polypeptide is recognized by two hydrophobic domains of the human Y4 receptor binding pocket. *J. Biol. Chem.* **289**, 5846–5859 (2014).
42. M. M. Gershkovich, V. E. Groß, O. Vu, C. T. Schoeder, J. Meiler, S. Prömel, A. Kaiser, Structural perspective on ancient neuropeptide Y-like system reveals hallmark features for peptide recognition and receptor activation. *J. Mol. Biol.* **433**, 166992 (2021).
43. B. Xu, H. Fällmar, L. Boukharta, J. Pruner, I. Lundell, N. Mohell, H. Gutiérrez-de-Terán, J. Åqvist, D. Larhammar, Mutagenesis and computational modeling of human G-protein-coupled receptor Y2 for neuropeptide Y and peptide YY. *Biochemistry* **52**, 7987–7998 (2013).
44. B. Xu, S. Vasile, S. Østergaard, J. F. Paulsson, J. Pruner, J. Åqvist, B. S. Wulff, H. Gutiérrez-de-Terán, D. Larhammar, Elucidation of the binding mode of the carboxyterminal region of peptide YY to the human Y_2 receptor. *Mol. Pharmacol.* **93**, 323–334 (2018).
45. S. Hoffmann, B. Rist, G. Videnov, G. Jung, A. G. Beck-Sickinger, Structure-affinity studies of C-terminally modified analogs of neuropeptide Y led to a novel class of peptidic Y_1 receptor antagonist. *Regul. Pept.* **65**, 61–70 (1996).
46. S. L. Pedersen, B. Holst, N. Vrang, K. J. Jensen, Modifying the conserved C-terminal tyrosine of the peptide hormone PYY3-36 to improve Y2 receptor selectivity. *J. Pept. Sci.* **15**, 753–759 (2009).
47. H. Akerberg, H. Fällmar, P. Sjödin, L. Boukharta, H. Gutiérrez-de-Terán, I. Lundell, N. Mohell, D. Larhammar, Mutagenesis of human neuropeptide Y/peptide YY receptor Y2 reveals additional differences to Y1 in interactions with highly conserved ligand positions. *Regul. Pept.* **163**, 120–129 (2010).
48. V. Thieme, N. Jolly, A. N. Madsen, K. Bellmann-Sickert, T. W. Schwartz, B. Holst, H. M. Cox, A. G. Beck-Sickinger, High molecular weight PEGylation of human pancreatic polypeptide at position 22 improves stability and reduces food intake in mice. *Br. J. Pharmacol.* **173**, 3208–3221 (2016).
49. D. N. Mastronarde, Automated electron microscope tomography using robust prediction of specimen movements. *J. Struct. Biol.* **152**, 36–51 (2005).
50. J. Zivanov, T. Nakane, B. O. Forsberg, D. Kimanius, W. J. H. Hagen, E. Lindahl, S. H. W. Scheres, New tools for automated high-resolution cryo-EM structure determination in RELION-3. *eLife* **7**, e42166 (2018).
51. A. Punjani, J. L. Rubinstein, D. J. Fleet, M. A. Brubaker, cryoSPARC:Algorithms for rapid unsupervised cryo-EM structure determination. *Nat. Methods* **14**, 290–296 (2017).
52. S. Q. Zheng, E. Palovcak, J.-P. Armache, K. A. Verba, Y. Cheng, D. A. Agard, MotionCor2: Anisotropic correction of beam-induced motion for improved cryo-electron microscopy. *Nat. Methods* **14**, 331–332 (2017).
53. K. Zhang, Gctf: Real-time CTF determination and correction. *J. Struct. Biol.* **193**, 1–12 (2016).
54. A. Kucukelbir, F. J. Sigworth, H. D. Tagare, Quantifying the local resolution of cryo-EM density maps. *Nat. Methods* **11**, 63–65 (2014).
55. K. Arnold, L. Bordoli, J. Kopp, T. Schwede, The SWISS-MODEL workspace: A web-based environment for protein structure homology modelling. *Bioinformatics* **22**, 195–201 (2006).

56. E. F. Pettersen, T. D. Goddard, C. C. Huang, G. S. Couch, D. M. Greenblatt, E. C. Meng, T. E. Ferrin, UCSF Chimera—A visualization system for exploratory research and analysis. *J. Comput. Chem.* **25**, 1605–1612 (2004).
57. P. Emsley, K. Cowtan, Coot: Model-building tools for molecular graphics. *Acta Crystallogr. D Biol. Crystallogr.* **60**, 2126–2132 (2004).
58. P. D. Adams, P. V. Afonine, G. Bunkóczi, V. B. Chen, N. Echols, J. J. Headd, L.-W. Hung, S. Jain, G. J. Kapral, R. W. Grosse Kunstleve, A. J. McCoy, N. W. Moriarty, R. D. Oeffner, R. J. Read, D. C. Richardson, J. S. Richardson, T. C. Terwilliger, P. H. Zwart, The Phenix software for automated determination of macromolecular structures. *Methods* **55**, 94–106 (2011).
59. V. B. Chen, W. B. Arendall III, J. J. Headd, D. A. Keedy, R. M. Immormino, G. J. Kapral, L. W. Murray, J. S. Richardson, D. C. Richardson, MolProbity: All-atom structure validation for macromolecular crystallography. *Acta Crystallogr. D Biol. Crystallogr.* **66**, 12–21 (2010).
60. E. Kostenis, Is Gα16 the optimal tool for fishing ligands of orphan G-protein-coupled receptors? *Trends Pharmacol. Sci.* **22**, 560–564 (2001).
61. M. P. Hall, J. Unch, B. F. Binkowski, M. P. Valley, B. L. Butler, M. G. Wood, P. Otto, K. Zimmerman, G. Vidugiris, T. Machleidt, M. B. Robers, H. A. Benink, C. T. Eggers, M. R. Slater, P. L. Meisenheimer, D. H. Klaubert, F. Fan, L. P. Encell, K. V. Wood, Engineered luciferase reporter from a deep sea shrimp utilizing a novel imidazopyrazinone substrate. *ACS Chem. Biol.* **7**, 1848–1857 (2012).
62. A. Kaiser, C. Hempel, L. Wanka, M. Schubert, H. E. Hamm, A. G. Beck-Sickinger, G protein preassembly rescues efficacy of $W^{6.48}$ toggle mutations in neuropeptide Y_2 receptor. *Mol. Pharmacol.* **93**, 387–401 (2018).

Acknowledgments: The cryo-EM studies of the NPY-Y_1R-G_{i1} and PP-Y_4R-G_{i1} complexes were performed at the EM facility of Shanghai Institute of Materia Medica (SIMM), Chinese Academy of Sciences. The cryo-EM data of the NPY-Y_2R-G_{i1} complex were collected at the Center for Biological Imaging (CBI), Institute of Biophysics, Chinese Academy of Sciences. We thank Q. Wang from SIMM and B. Zhu from CBI for their help with cryo-EM data collection. **Funding:** This work was supported by the following funding: National Science Foundation of China grants 31825010 (B.W.), 82121005 (B.W.), and 32161133011 (Q.Z.); National Key R&D Program of China 2018YFA0507000 (B.W. and Q.Z.); CAS Strategic Priority Research Program XDB37030100 (B.W. and Q.Z.); Shanghai Science and Technology Committee grant 19JC1416200 (B.W.); Shanghai Pilot Program for Basic Research—Chinese Academy of Sciences, Shanghai Branch JCYJ-SHFY-2021-008 (B.W.); and Deutsche Forschungsgemeinschaft (DFG, German Research Foundation), project number 421152132, SFB 1423/1, subproject A04; B01 (A.G.B.-S.) and B03 (A.K.). **Author contributions:** T.T. optimized the constructs, developed the expression and purification procedures, prepared the protein samples for cryo-EM, performed signaling assays, and helped with manuscript preparation. Q.T. performed signaling assays and negative-stain EM data acquisition and analysis. S.H. prepared cryo-sample, collected cryo-EM data, and performed cryo-EM data processing and analysis, model building, and structure refinement. A.K. and C.S. developed the NanoBRET assays. K.L., A.D., V.B., and K.M. cloned the receptor mutants and performed functional studies. A.D., C.S., and A.K. performed the NanoBRET assays. H.W. helped with signaling assays. M.W. performed the 3D variability analysis. X.C. and C.Y. expressed the proteins. M.K., J.K., and S.R.-R. helped with data analysis/interpretation and edited the manuscript. J.K. provided peptide ligands for Y_2R construct optimization and ligand screening. A.G.B.-S. and A.K. oversaw the NanoBRET assay, helped with data analysis/interpretation, and edited the manuscript. B.W. and Q.Z. initiated the project, planned and analyzed experiments, supervised the research, and wrote the manuscript with input from all coauthors. **Competing interests:** J.K. and S.R.-R. are employees of Novo Nordisk A/S, and S.R.-R. is also a shareholder of Novo Nordisk A/S. The other authors declare that they have no competing interests. **Data and materials availability:** Atomic coordinates and cryo-EM density maps for the structures of NPY-Y_1R-G_{i1}, NPY-Y_2R-G_{i1}, and PP-Y_4R-G_{i1} have been deposited in the RCSB Protein Data Bank (PDB) with identification codes 7X9A, 7X9B, and 7X9C, and the Electron Microscopy Data Bank (EMDB) under accession codes EMD-33069, EMD-33070, and EMD-33071. All other data are available in the main text or the Supplementary Materials.

Submitted 27 August 2021
Accepted 21 March 2022
Published 4 May 2022
10.1126/sciadv.abm1232